batteries

*Review*

# Heteroatom Doping Strategy of Advanced Carbon for Alkali Metal-Ion Capacitors

**Ti Yin, Yaqin Guo, Xing Huang *, Xinya Yang, Leixin Qin, Tianxiang Ning, Lei Tan, Lingjun Li and Kangyu Zou ***

School of Materials Science and Engineering, Changsha University of Science and Technology, Changsha 410114, China; 202228020409@stu.csust.edu.cn (T.Y.); 202228020413@stu.csust.edu.cn (Y.G.); 202328020426@stu.csust.edu.cn (X.Y.); 202328020438@stu.csust.edu.cn (L.Q.); ningtianxiang@csust.edu.cn (T.N.); tanlei@csust.edu.cn (L.T.); lingjun.li@csust.edu.cn (L.L.)

* Correspondence: 22206031250@stu.csust.edu.cn (X.H.); ky-zou@csust.edu.cn (K.Z.)

**Abstract:** Alkali metal-ion capacitors (AMICs) combine the advantages of the high specific energy of alkali metal-ion batteries (AMIBs) and the high power output of supercapacitors (SCs), which are considered highly promising and efficient energy storage devices. It is found that carbon has been the most widely used electrode material of AMICs due to its advantages of low cost, a large specific surface area, and excellent electrical conductivity. However, the application of carbon is limited by its low specific capacity, finite kinetic performance, and few active sites. Doping heteroatoms in carbon materials is an effective strategy to adjust their microstructures and improve their electrochemical storage performance, which effectively helps to increase the pseudo-capacitance, enhance the wettability, and increase the ionic migration rate. Moreover, an appropriate heteroatom doping strategy can purposefully guide the design of advanced AMICs. Herein, a systematic review of advanced heteroatom (N, S, P, and B)-doped carbon, which has acted as a positrode and negatrode in AMICs (M = Li, Na, and K) in recent years, has been summarized. Moreover, emphasis is placed on the mechanism of single-element doping versus two-element doping for the enhancement in the performance of carbon positrodes and negatrodes, and an introduction to the use of doped carbon in dual-carbon alkali metal-ion capacitors (DC-AMICs) is discussed. Finally, an outlook is given to solve the problems arising when using doped carbon materials in practical applications and future development directions are presented.

**Keywords:** alkali metal-ion capacitor; carbon material; heteroatom doping; electrochemical performance

check for updates

Academic Editor: George Zheng Chen

Received: 26 December 2024
Revised: 3 February 2025
Accepted: 6 February 2025
Published: 8 February 2025

**Citation:** Yin, T.; Guo, Y.; Huang, X.; Yang, X.; Qin, L.; Ning, T.; Tan, L.; Li, L.; Zou, K. Heteroatom Doping Strategy of Advanced Carbon for Alkali Metal-Ion Capacitors. *Batteries* **2025**, *11*, 69. https://doi.org/10.3390/batteries11020069

**Copyright:** © 2025 by the authors. Licensee MDPI, Basel, Switzerland. This article is an open access article distributed under the terms and conditions of the Creative Commons Attribution (CC BY) license (https://creativecommons.org/licenses/by/4.0/).

## 1. Introduction

The evolution of energy storage technology has led to increased demands for advanced energy storage devices that offer higher energy and power densities, along with extended lifecycles. Constructing such advanced energy storage devices is crucial for the efficient utilization and storage of sustainable energy sources. Currently, lithium-ion batteries (LIBs) and supercapacitors (SCs) dominate the energy storage market [1]. However, LIBs, characterized by their low specific power, and SCs, characterized by their low specific energy, are increasingly unable to meet the escalating energy demands of the market for energy storage technologies [2–4]. In 2001, Amatucci et al. [5] reported lithium-ion capacitors (LICs) for the first time, which are constructed by an activated carbon (AC) positrode and a $Li_4Ti_5O_{12}$ (LTO) negatrode. Surprisingly, LICs exhibit a specific energy three times greater than that of conventional SCs (20 Wh $kg^{-1}$), heralding a new era in energy storage systems. LICs combine SC-type positrodes and LIB-type negatrodes [6], achieving high

specific energy/power and a long lifecycle. Compared to lithium, which is present in low concentrations (0.002wt.%), sodium (2.36wt.%) and potassium (2.09wt.%) are more abundant on Earth and exhibit analogous chemical properties to lithium. They demonstrate significant potential for large-scale storage and cost-effectiveness. Therefore, sodium-ion capacitors (SICs) and potassium-ion capacitors (KICs) exhibit similar mechanisms to LICs, which have become one of the most promising electrochemical energy storage devices. The relationship between the specific energy and specific power of common electrochemical energy storage devices is depicted in Figure 1a [7]. Electrode materials play a crucial role in the electrochemical performance of alkali metal-ion capacitors (AMICs) [8]. Carbon materials, known for their low cost, large specific surface area, and excellent electrical conductivity, are used as electrode materials in AMICs to store energy by absorbing electrolyte ions on the electrode surface, forming an electric double-layer structure. Nevertheless, the application of carbon materials is still constrained due to their low specific capacity, limited kinetic performance, and scarcity of active sites, which result in the inferior specific energy of the assembled devices [9,10].

Heteroatom doping is a rational design method, used in the realm of advanced material development, involving the substitution of certain carbon atoms with other elements [11–14]. This process can alter the electronic structure of the carbon matrix, thereby promoting charge transfer [15]. Additionally, it can increase the number of redox-active sites and defect locations, as well as expand the interlayer distance within the carbon structure. Doping with various heteroatoms can further enhance specific physical and chemical properties of carbon materials, such as electrical conductivity and surface wettability [16,17]. Superior electrical conductivity ensures the swift passage of electrical currents through the material, while excellent surface wettability fosters stronger interactions between the material and its surrounding environment. Figure 1b,c [18] illustrate the comparative positive and negative impacts of different doping atoms in batteries and SCs, respectively. In the context of AMICs, carbon negatrodes and carbon positrodes operate through distinct energy storage mechanisms. For carbon negatrodes, specific heteroatom doping may be essential to bolster stability and energy storage capacity, whereas for carbon positrodes, a different type of heteroatom doping might be necessary to enhance conductivity and reactivity. Consequently, their doping modification strategies and performance enhancement pathways can differ significantly.

Selecting the right dopant atoms is a critical research area for researchers, as it can significantly enhance the electrochemical performance of battery-type carbon negatrodes and capacitor-type carbon positrodes in a targeted manner. This review offers a systematic examination of the recent advancements in the use of advanced heteroatom (N, S, P, and B)-doped carbons as both positrodes and negatrodes in AMICs (M = Li, Na, and K). It concentrates on the application of single-element-doped and double-doped carbons in AMICs, delivering a thorough analysis of the distinct performance benefits offered by various elemental doping strategies and elucidating the mechanisms behind performance enhancement. Furthermore, this discussion tackles the challenges that doped carbon materials face in practical applications and proposes potential avenues for future research and development. The aim is to improve the performance of LICs, SICs, and KICs, and by extension, other MICs. By identifying the unique advantages and mechanisms of different doping elements, researchers can better tailor the design of carbon materials to meet the specific demands of high-performance energy storage devices.

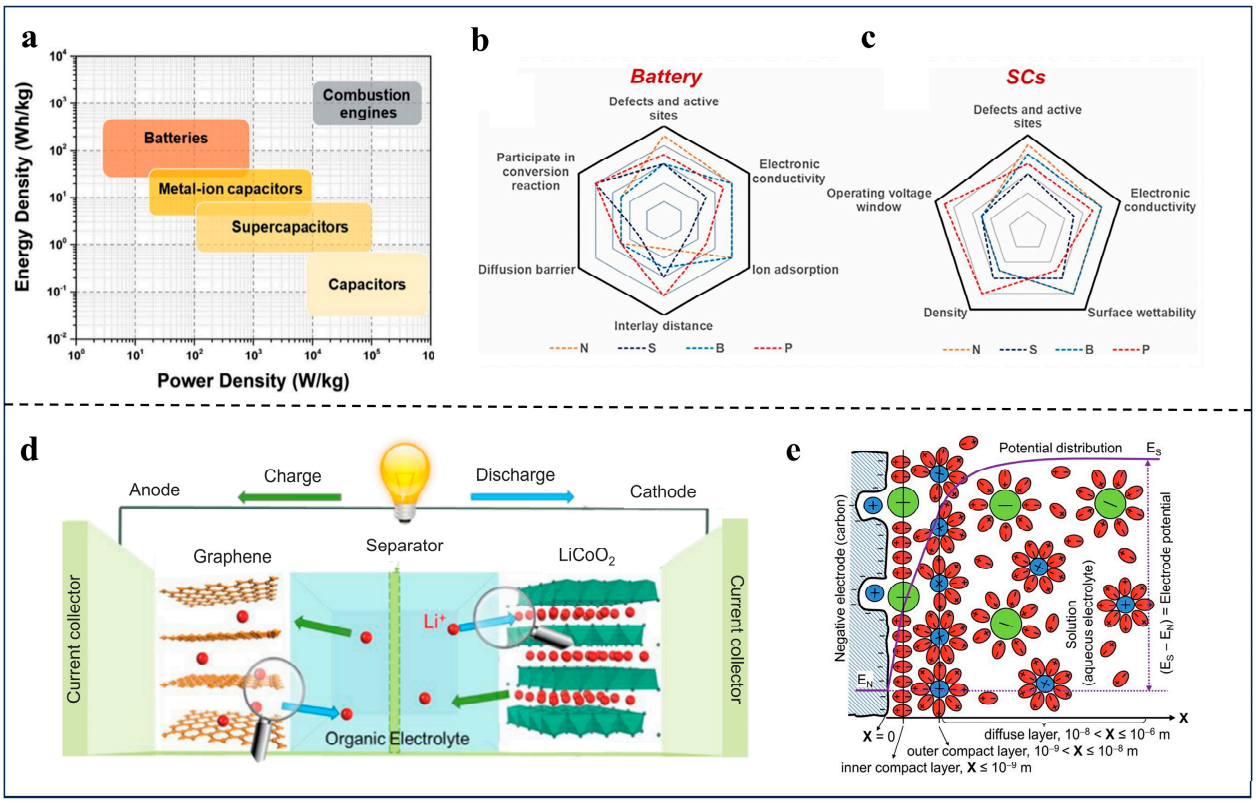



**Figure 1.** (**a**) A Ragone diagram of the energy storage devices as indicated. Reproduced with permission from Ref. [7]. Copyright 2022, The Royal Society of Chemistry. A comparison of the positive and negative effects of the doping of different heteroatoms in (**b**) batteries and (**c**) SCs. Reproduced with permission from Ref. [18]. Copyright 2021, The Royal Society of Chemistry. (**d**) A schematic of the charging and discharging process in typical MIBs. Reproduced with permission from Ref. [19]. Copyright 2019, Wiley. (**e**) Schematic representations of the EDL structure (cross-section) of the interface between a porous-carbon negative electrode and an aqueous electrolyte. Reproduced with permission from Ref. [20]. Copyright 2017, Taylor & Francis.

## 2. Energy Storage Mechanisms in Electrochemical Storage Devices

AMICs are hybrid energy storage devices that integrate the energy storage mechanisms of both AMIBs and SCs. Typically, an AMIC comprises a battery-type negatrode and a capacitor-type positrode. The battery-type negatrode supplies sustained power to the device, while the capacitive positrode is designed for the swift absorption and release of energy. MICs are characterized by their high energy and power densities, as well as their extended operational lifetimes. However, there is a kinetic rate mismatch between the $Li^+$ intercalation/de-intercalation of the battery-type negatrode and the ion adsorption/desorption behavior of the capacitor-type negatrode. Thus, it is necessary to understand the two different energy storage mechanisms to ensure the rational engineering of carbon materials for advanced AMICs.

### *2.1. Embedding–Removal Mechanism of AMIBs*

Rechargeable AMIBs have indeed become prominent contenders in the realm of new energy technologies, offering portability, energy efficiency, and environmental sustainability. The energy storage in AMIBs is predicated according to the reversible intercalation/de-intercalation of alkali metal ions ($M^+$) within the electrode materials, a process often referred to as the "rocking chair" mechanism. This mechanism is aptly likened to a magical rocking chair, where $M^+$ oscillates between the negatrode and positrode materials during the charging and discharging cycles.

Let us take lithium-ion batteries (LIBs) as an example. Figure 1d [19] shows the charge–discharge process of a conventional lithium-ion battery. During charging, electrons follow the external circuit from the positive electrode to the negative electrode, while $Li^+$ located in the lithium layer undergoes removal and enters the electrolyte. Firstly, $Li^+$ is dissolved by the solvent molecules in the electrolyte, and then migrates across the separator to the negatrode under the action of the electric field to undergo de-solvation behavior and is intercalated in the graphite layer. The discharge process of a lithium-ion battery is opposite to the charging process; electrons flow from the negative electrode to the positive electrode, and $Li^+$ is removed from the graphite and finally intercalated in the positive electrode.

There exists a significant correlation between the reversible intercalation/de-intercalation properties of AMIBs and their specific energy. If the electrode material possesses a limited number of sites that restrict the quantity of $M^+$ that can be stored, this limitation diminishes the amount of energy that can be released by the AMIB, resulting in reduced specific energy. Conversely, unfavorable external conditions, such as temperature, pressure, and electrolyte environment, can also impact these reversible intercalation/de-intercalation properties, thereby affecting the specific energy of the battery.

### 2.2. Electric Double-Layer Capacitors

Electric double-layer capacitors (EDLCs), a subset of supercapacitors, play a critical role in modern energy storage solutions. Based on the electrical double-layer model shown in Figure 1e [20], EDLCs store electrical energy through electrostatic interactions, which facilitate charge separation within the Helmholtz double layer at the interface between the electrode surface and the electrolyte [21–23]. When subjected to an electric field, the positive and negative ions in the electrolyte migrate toward the respective oppositely charged electrodes, creating an electric double layer on the electrode surfaces that enables charge storage [24,25]. During the charging phase, anions migrate to the negatrode, while cations move toward the positrode. Conversely, during the discharging phase, these ions move in the opposite direction, releasing the stored charge.

Table 1 presents a comparison of the primary performance metrics of commercialized AMIBs, SCs, and AMICs. It is evident that EDLCs, a type of SC, exhibit superior specific power and cycling stability in comparison to AMIBs [26,27]. EDLCs store energy through a non-Faradaic process that does not involve electron transfer or redox reactions. This distinct energy storage mechanism endows EDLCs with higher efficiency and stability during both the energy storage and release processes. Consequently, double-layer capacitors can serve as an alternative or supplement to secondary rechargeable batteries in applications where high power transfer or rapid energy harvesting is necessary.

**Table 1.** Comparison of main properties of commercialized AMIBs, SCs, and AMICs [26,27].

| Properties | AMIB | SC | AMIC |
|---|---|---|---|
| Discharging time | 0.3–3 h | ~30 s | min to h |
| Charging time | 1–5 h | s to min | min to h |
| Specific energy (Wh $kg^{-1}$) | 150–250 | 20–30 | 20–200 |
| Specific power (W $kg^{-1}$) | <1000 | 500–10,000 | 100–20,000 |
| Cycling efficiency (%) | 70–85 | 85–98 | 70–95 |
| Lifecycle (Cycles) | <4000 | >500,000 | >25,000 |

## 3. Element Doping for Carbon Negatrode

The carbon negatrode, known for its abundant availability, high conductivity, and stability, is a key component in many energy storage systems. Graphite, the most common negatrode material for lithium-ion batteries, has a theoretical specific capacity of

372 mAh $g^{-1}$. Since $Na^+$ has a larger ionic radius than $Li^+$, it cannot be intercalated or de-intercalated between graphite layers. Consequently, amorphous carbon with significant disorder is employed for its negative electrode [28], among which hard carbon is widely utilized due to its high theoretical specific capacity (>300 mAh $g^{-1}$) [29]. In contrast, potassium can form intercalation compounds with graphite, allowing graphite to serve as a negatrode material for potassium-ion batteries that exhibit a high theoretical capacity of 279 mAh $g^{-1}$ and demonstrate considerable potassium-embedding capabilities. However, its theoretical capacity, which stands at 372 mAh $g^{-1}$, and its suboptimal rate performance are limitations that prevent it from meeting the specific energy and specific power demands expected from AMICs. During rapid charging and discharging cycles, carbon negatrodes struggle to respond swiftly to fluctuations in current, further highlighting their inability to fulfill the specific energy and specific power requirements of AMICs. Within the electrochemical energy storage processes of AMICs, there is a significant mismatch between the slow ion diffusion at the negatrode and the rapid electrostatic accumulation at the positrode [30–33], leading to an imbalance in negatrode/positrode kinetics. Therefore, it is necessary to strategically develop carbon negatrodes with high multiplicity performance [34–36], which will increase the specific energy and specific power of AMICs at the same time.

### 3.1. N Doping

Nitrogen, as the most widely studied doping element, is easier to chemically bond with carbon compared to other elemental doping. The atomic radius of nitrogen is slightly smaller than that of carbon, which means that doping with nitrogen results in minimal disruption to the backbone structure of the carbon material, thereby preserving its stability [37]. Nitrogen atoms tend to form new micropores in the carbon skeleton and increase the specific surface area of the material [38]. In addition, the electronegativity of the nitrogen atoms is high (N is 3.04 and C is 2.55), generating very small lattice distortions [39,40], which gives doped carbon materials excellent electrical conductivity [41].

There are five types of doped N (Figure 2a), namely pyrrolic N, nitroso group, amino group, pyridinic N, and graphitic N [42,43]. Positively charged pyridinic N oxides and graphite N elevate electrical conductivity and facilitate electron transport within the carbon electrode. Negatively charged pyridinic N and pyrrolic N generate pseudo-capacitance and enhance the specific capacity and rate performance of the negatrode carbon material [44]. Despite these benefits, nitrogen doping is not without its drawbacks; for instance, graphitic N can diminish the cycling stability and initial coulombic efficiency (ICE) of doped carbon materials. Thus, the choice of nitrogen doping type and quantity is of paramount importance. Tang et al. [45] developed a method to synthesize high-nitrogen-doped, low-graphitic-N carbons (LGNCs) that exhibit improved ICE by eliminating graphitic nitrogen from graphitic carbon nitride (g-$C_3N_4$) through a denitrification process. As shown in Figure 2b, the LGNC (C:N = 4:1) has higher pyridinic N and pyrrolic N contents and a lower graphitic N content compared to the other two LGNCs (2:1 and 8:1). Therefore, it shows excellent lithium storage capacity and good cycle stability. By calculating the contribution of LGNC diffusion (intercalation) and capacitance (surface-controlled) at different scanning rates (Figure 2c,d), it is evident that the capacitive contribution of LGNC is directly proportional to the scanning rate.

Incorporating nitrogen into the graphite structure of carbon nanomaterials, such as graphene, carbon nanotubes, and activated carbon, can significantly enhance the atomic and electronic structure of these substrates. This modification not only boosts their electrical conductivity but also introduces a conjugated carbon system with sp2 hybridization. These changes can markedly alter the properties of the material, including its reactivity,

mechanical strength, and electrocatalytic performance. Zhao et al. [46] utilized $N_2$ gas as a dopant to achieve in situ nitrogen doping of carbon substrates. The Raman spectroscopy results indicate a progressive decrease in the intensity ratio ($I_D/I_G$) of the D-band to the G-band as gaseous $N_2$ is introduced (Figure 2e). Additionally, a two-dimensional band near 2669 $cm^{-1}$ emerged in the spectra of C-N-30-8 h (introducing $N_2$ with a flow rate of 30 $mL \cdot min^{-1}$ for 8 h), demonstrating high crystallinity and intensity within the range of 1000–3000 $cm^{-1}$ [47,48]. This suggests that the doping of N atoms enhances the graphitization of the carbon material, which in turn improves the sodium storage capabilities of C-N-30-8h at high rates.

Furthermore, nitrogen doping in carbon negatrodes enhances the anion-exchange capacity [49], creates additional defects and active sites, and bolsters the catalytic activity of redox reactions [50–52], which in turn improves the specific capacitance [53–57]. For instance, the introduction of substantial nitrogen content significantly boosts the pseudo-capacitance contribution of reticulated nitrogen-doped carbon nanosheets' negatrode, which stands at 58.5%, compared to the 38.3% contribution from carbon nanosheets' negatrode without nitrogen doping [58]. The researchers [59] induced graphite nanodomains and micro mesopores into N-doped carbon to prepare tubular N-doped porous carbons (NPCs), called $As_8Mg$. As shown in Figure 2f, $As_8Mg$ exhibits a capacity retention rate of up to 98.7% with close to 100% CE at a specific current of 0.2 A $g^{-1}$. The cycling performance of $As_8Mg$ is exceptionally outstanding among a variety of NPC negatrodes. Based on $As_8Mg$, SICs also achieve high specific energy (51 Wh $kg^{-1}$) and specific power (10,410 W $kg^{-1}$). This indicates that N-doped $As_8Mg$ has high capacitive energy storage properties and is one of the ideal negatrodes for sodium-ion capacitors.

Nitrogen doping exerts a substantial influence on the storage of metal ions, with a particular emphasis on three forms of doped nitrogen: pyrrolic N, pyridinic N, and graphitic N. Taking $Li^+$ as an example, Chen et al. [60] prepared nitrogen-doped interconnected carbon networks (INCs) which revealed high reversible capacity and excellent electrochemical kinetics. The prepared INC//AC LIB has high specific energy (172 Wh $kg^{-1}$ at 260 W $kg^{-1}$) and large specific power (26 kW $kg^{-1}$ at 108 Wh $kg^{-1}$). The XPS results showed that the N element of the INCs prepared at 800 °C is mainly divided into three components: pyridinic N (N-6, 398.4 eV), pyrrolic N (N-5, 400.2 eV), and graphitic N (N-Q, 401.2 eV) (Figure 2g). Among the N-doped structures, the study concludes that the electronic defects of pyrrolic N (N-5) and pyridinic N (N-6) enhance the adsorption of Li atoms [61,62], while graphitic N doping (N-Q) weakens the adsorption of Li atoms.

### *3.2. S Doping, P Doping, and B Doping*

Owing to the larger atomic radius of sulfur, sulfur doping may occupy a larger space in the pore volume. This causes the expansion of layer spacing and a significant decrease in the specific surface area of the carbon material [63]. Sulfur-doped carbon typically results in larger defects, distortions, and increased interlayer distances within the carbon structure [64–67]. S atoms are often found at the edges or defects of carbon planes, which can offer a greater number of active sites. Using the synthetic strategy of extracting sulfur-doped carbon flakes from softwood (Figure 3a), Casal and co-workers produced S-doped carbon flakes used as negatrodes for SICs [68]. The Galvanostatic charge–discharge (GCD) potential curves in Figure 3b indicate that for S-doped carbon sheets at discharge potentials of 1.2–1.5 V, the curve lengths are proportional to the sulfur content. Meanwhile, the GCD curve of the undoped sheets (Figure 3c) has a potential plateau below 0.1 V. The addition of sulfur doubles the CS-700m (prepared at 700 °C, in the absence of sulfur and subjected as well to a ball milling process) capacity, providing an excellent performance at 420 mAh $g^{-1}$ (403 mAh $cm^{-3}$, ICE = 69%). At a high rate of 10 A $g^{-1}$ (Figure 3d), the S-doped carbon

sheets (55–40 mAh $g^{-1}$) possess a significantly larger reversible capacity (15 mAh $g^{-1}$) than the undoped carbon sheet, indicating that the redox reaction brought about by sulfur can still play a significant role at high rates. The above results suggest that sulfur doping provides abundant vacant defect locations for the carbon sheets. Due to the defects, the interlayer spacing of carbon is increased [69], and the resistance to $Na^+$ diffusion is greatly reduced, accelerating its embedding/removal time.

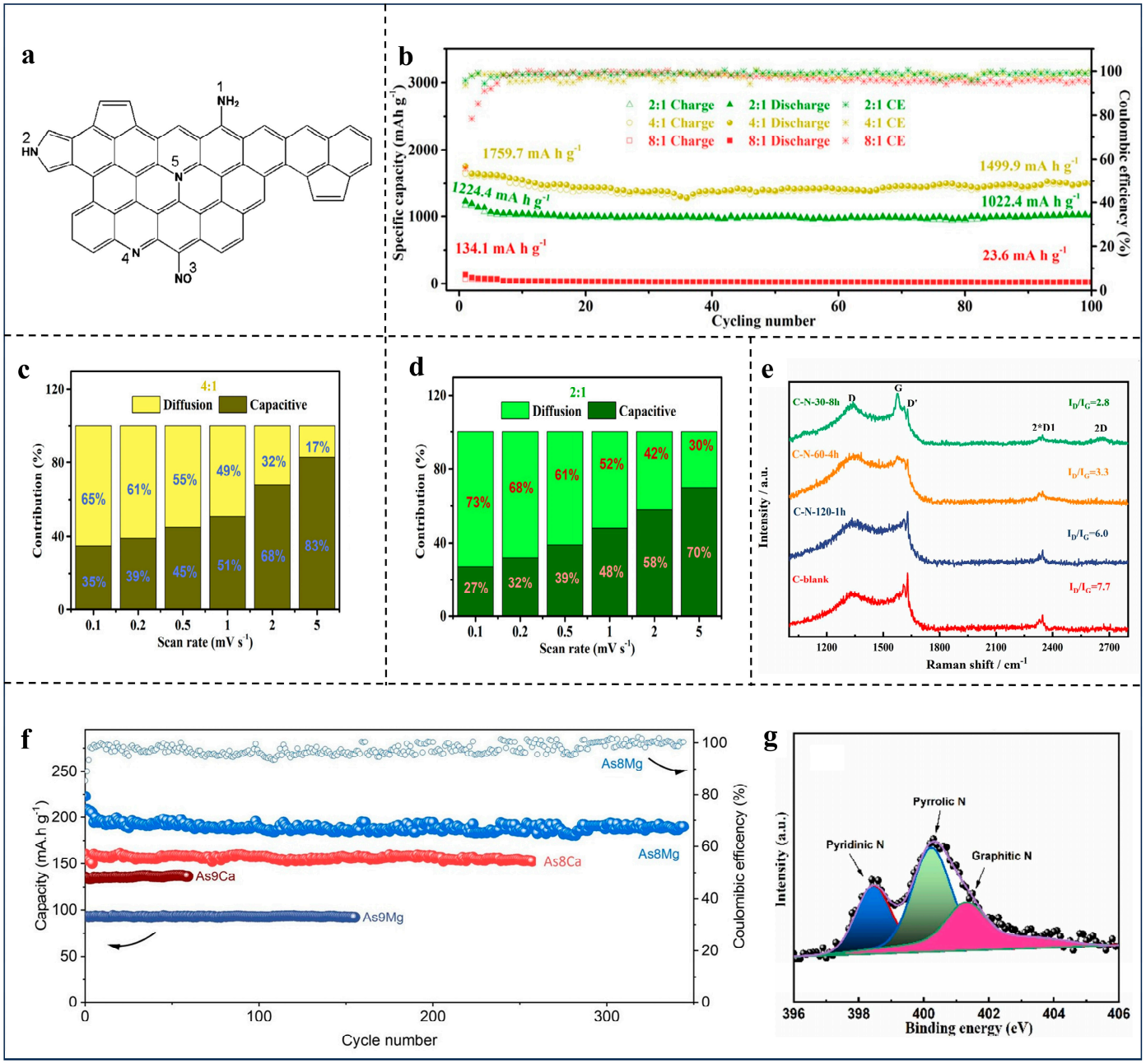



**Figure 2.** (**a**) Schematic overview of possible N sites of carbon backbone. Reproduced with permission from Ref. [43]. Copyright 2010, The Royal Society of Chemistry. (**b**) Galvanostatic charge/discharge cycling performances. Contribution of capacitive and diffusion-controlled capacity for LGNC at (**c**) 4:1 and (**d**) 2:1. LGNC, low-graphitic-N carbon. Reproduced with permission from Ref. [45]. Copyright 2022, Wiley. (**e**) Raman spectra of C-blank, C-N-120-1h, C-N-60-4h, and C-N-30-8h. Reproduced with permission from Ref. [46]. Copyright 2023, Elsevier. (**f**) Cycling performance of samples with specific current of 0.2 A·$g^{-1}$. Reproduced with permission from Ref. [59]. Copyright 2024, Wiley. (**g**) High-resolution XPS for N1s of INC prepared at 800 °C. Reproduced with permission from Ref. [60]. Copyright 2023, Elsevier.

Phosphorus (P) atoms are regarded as one of the most promising doping elements. Compared to nitrogen, which shares the same number of valence electrons, P atoms have a larger radius (~0.110 nm). Therefore, phosphorus atoms will cause pore enlargement and increase pore spacing during the doping process [70]. This characteristic endows phosphorus-doped carbon with significant structural distortions and a robust adsorption capacity for $M^+$ [71–74]. Yang et al. [75] successfully synthesized phosphorus-doped hard carbon (PHC-4), which contains a substantial amount of phosphorus (3.44%), through esterification and carbonation reactions between starch and phytic acid. PHC-4 is based on the phytic acid volume of 4 mL. PHC-4 has three main components. $Li_xPC_y$ with P-C bonds is involved in the electrochemical redox reaction and provides high-capacitance performance [76]; meanwhile, P-O and P=O bonds enhance the adsorption of $M^+$ by the carbon material [77]. The binding of phosphorus atoms and active sites of carbon increases the chemical stability. Moreover, it is conducive to the insertion/extraction of $Li^+$, and the presence of P-doped atoms inhibits the oxidation of the carbon materials [78].

Boron (B) doping can significantly alter the characteristics of carbon-based materials in several ways: It disrupts the electroneutrality of these materials, leading to the generation of numerous active sites [79,80], and it also manages the charge distribution, which in turn expedites electron transfer [81,82]. Moreover, B doping can substitute for carbon atoms within the structure of the material, altering its electronic configuration and introducing more micropores into the carbon skeleton [83,84]. These modifications result in improved electrochemical performance for B-doped carbon in supercapacitors. Researchers [85] prepared boron-doped graphene nanosheets (BGNSs) by incorporating B into graphene nanosheets. B doping indispensably boosted the unique lithium storage mechanism and the adsorption properties of microporous capacitive carbon in BGNS. As shown in Figure 3e of the pore size distributions (PSDs), the addition of B prevented the agglomeration of graphene sheets. Moreover, it induced the formation of p-type conductive networks [86,87]. The mesoporous structure of BGNS observed in TEM images (Figure 3f) also supported the above conclusion. Meanwhile, the lithiation/de-lithiation ability of BGNS was greatly enhanced compared to undoped TGNS, as shown in Figure 3g. This enhancement is likely a result of boron doping increasing the disorder within the matrix, which in turn promotes porosity and the creation of $Li^+$ storage sites.

### *3.3. N/S Co-Doping*

N/S co-doped carbon has seen rapid development in recent years, capitalizing on the synergistic effects between nitrogen and sulfur. The co-doping of N and S atoms enhances the conductivity of carbon materials, increases interlayer distances, and introduces more defect sites within the carbon structure. These changes lead to an improved reversible storage capacity and rate capability, enhancing the overall performance of $M^+$ ion storage [88–91]. Researchers [92] synthesized an N/S double-doped multistage porous carbon (NSC) with excellent reversibility. Based on this premise, the highly stable LIC (Figure 3h) constructed achieves both high specific energy and high specific power simultaneously. As shown in the XPS spectrum (Figure 3i), the N1 peaks of NSC1–3 include pyridinic N, pyrrolic N, graphitic N, and nitrogen-containing oxides [93,94]. Among these, pyridinic N and pyrrolic N demonstrate strong adsorption properties for $M^+$, such as $Li^+$ and $Na^+$, due to their electron-deficient characteristics [95]. Additionally, S doping enhances the surface wettability of the carbon material and the electrolyte, facilitating rapid charge transfer [96,97]. Moreover, the incorporation of both N and S doping in porous carbon significantly reduces interfacial resistance, thereby improving electron conduction [98,99]. The presence of nitrogen and sulfur heteroatoms contributes to superior sodium-ion storage capabilities, allowing carbon negatrodes doped with N/S to achieve a high reversible

capacity and exhibit remarkable cycle stability. As a result, N/S-doped carbon has been widely utilized as a negatrode in SICs [100–106].

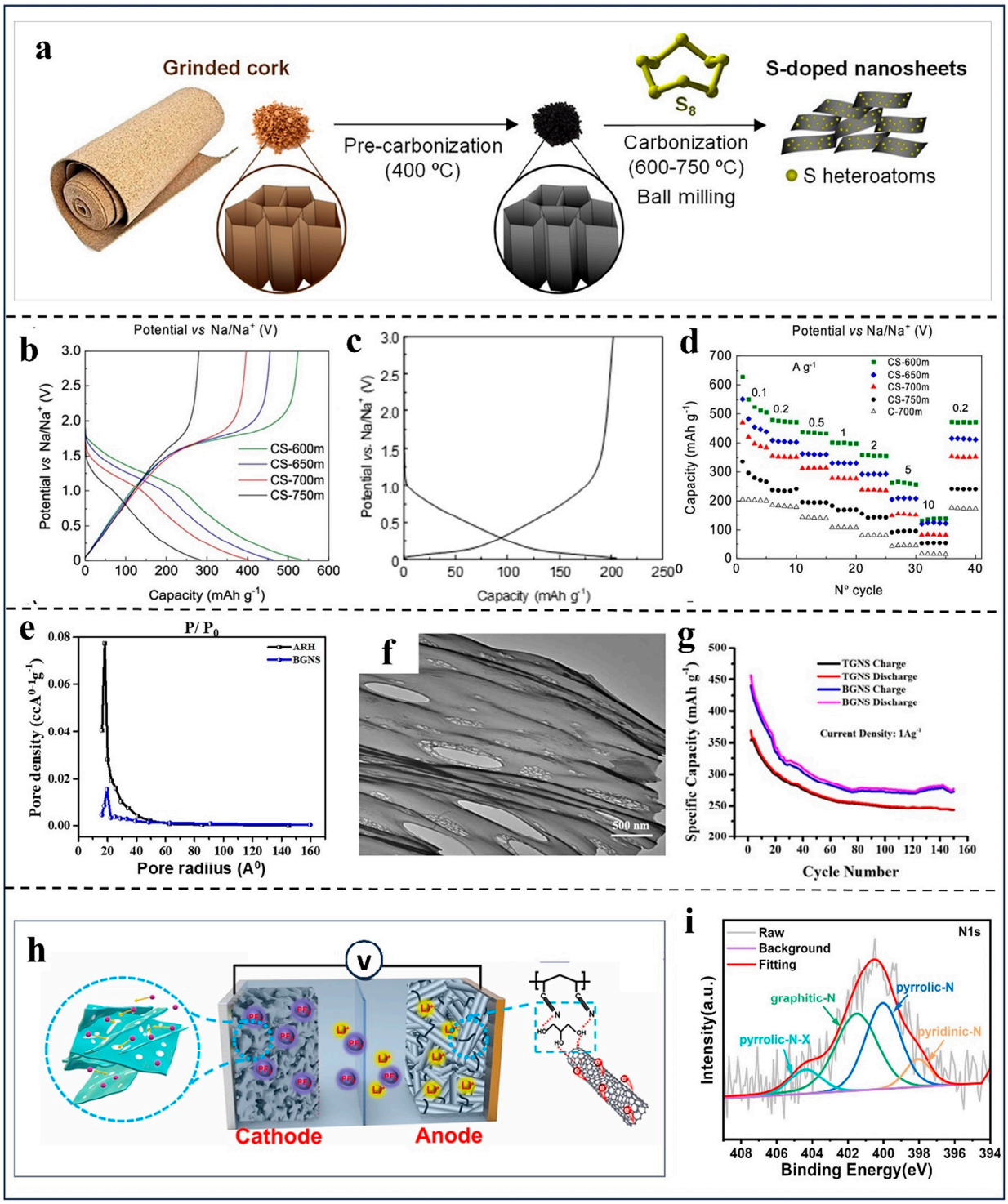



**Figure 3.** (**a**) An illustration of the synthesis strategy of S-doped carbon sheets from cork. (**b**,**c**) GCD profiles in the third cycle for the different S-doped sheets and un-doped carbon sheets C-700m. (**d**) The rate capability of the different S-doped sheets. Reproduced with permission from Ref. [68]. Copyright 2023, American Chemical Society. (**e**) Pore size distribution plot of BGNSs and ARH. (**f**) TEM images of BGNSs. (**g**) Cycling of BGNSs and TGNSs at a specific current of 1 A $g^{-1}$. Reproduced with permission from Ref. [85]. Copyright 2022, Elsevier. (**h**) A schematic illustration of LIC (NSC//GPN@CNTs). (**i**) N1s Entire XPS spectra of NSC1–3 carbonized at 800 °C. Reproduced with permission from Ref. [92]. Copyright 2023, Elsevier.

## 4. Element Doping for Carbon Positrode

The capacitance of metal-ion capacitors is often limited by the properties of the positrode material, making the selection of a suitable positrode material a critical decision. Carbon, being the most prevalent positrode material, is known for its significant capacitance contribution to fast ion storage and its excellent chemical stability, which allows it to maintain its structure and performance across a broad spectrum of electrolyte environments. However, the low specific capacity of carbon can lead to reduced specific energy in devices that incorporate it. Consequently, researchers have dedicated considerable effort to designing positrode carbon materials with enhanced specific capacity. There is an ongoing quest to discover new electrode material structures and preparation techniques aimed at surmounting the challenges related to the low specific capacity of carbon materials. This continuous exploration is essential for advancing the performance and specific energy of AMICs.

### *4.1. N Doping*

To achieve a balance between electrochemical kinetics and specific capacity in the negatrode and positrode of AMICs, Xu and colleagues proposed a preparation method, combining the advantages of elemental doping and nanostructure, and also successfully prepared nitrogen-doped (3.65%) multistage porous carbon sphere (NHPCS) positrodes [107]. Nitrogen doping endows the NHPCS electrode with superior wettability compared to other electrodes, as shown in Figure 4a. This improved wettability is anticipated to reduce interfacial impedance, thereby enhancing the rate performance. Furthermore, Figure 4b illustrates that the synergistic effect of N/O doping markedly enhances the electrochemical performance of the NHPCS. The unique electronic configuration of nitrogen allows N-doped carbon materials to more readily attract ions from the electrolyte [108], which in turn boosts their capacitive characteristics.

### *4.2. N/S Co-Doping and N/B Co-Doping*

The introduction of different dopants into materials can significantly alter their electrochemical properties, leading to substantial changes in both physical and chemical characteristics [109]. Among these dopants, N is the most extensively used and is often co-doped with other elements to achieve synergistic effects, such as in the case of N/S co-doping. Recently, Shi et al. [110] prepared S/N co-doped porous carbon (SNC) by using a simple method. The addition of S and N enhanced the specific capacity and wettability of the SNC samples. The ratio of S to N can be fine-tuned to achieve the optimal synergistic effect, including on the pore structure of the resulting materials. Table 2 confirms the small pore sizes of SNC-3 and SNC-4 micropores. Simultaneously, as can be seen in the CV curves of Figure 4c, all SNC electrodes, particularly SNC-3, exhibit excellent capacitive behavior [111,112]. This is due to the ability of S to significantly enhance the reactivity between the electrode and the electrolyte. However, with an increase in S content and a corresponding decrease in carbon content, the specific capacity of SNC-4 diminishes, preventing the achievement of optimal performance. Therefore, the proportion of non-metallic elements in the doped material can be easily adjusted by modifying the ligand ratio to optimize performance. As depicted in Figure 4d, the LIC using SNC-3 as a positrode and pre-lithiation HC as a negatrode still outperforms others, and it can achieve powerful performance with maximum specific power (6072 W $kg^{-1}$) and maximum specific energy (52 Wh $kg^{-1}$).

The electronegativity of carbon lies between that of B and N, which makes it a versatile element for doping. By substituting some carbon atoms with N and B, the surface polarity and electronic structure of the carbon substrate can be synergistically modulated.

Consequently, co-doped carbon materials exhibit greater catalytic and electrochemical activity compared to their singly doped counterparts [113–118]. Zhang et al. [119] utilized N/B co-doped swollen reduced oxidized graphite (NBEG) as a positrode for SICs; the preparation process is shown in Figure 4e. N-containing functional groups are beneficial for increasing the electronic conductivity of carbon-based materials, inducing the creation of unbalanced charged regions in the carbon materials. This action not only enhances electronic conductivity but also provides additional active sites [120], thereby improving the overall electrochemical performance.

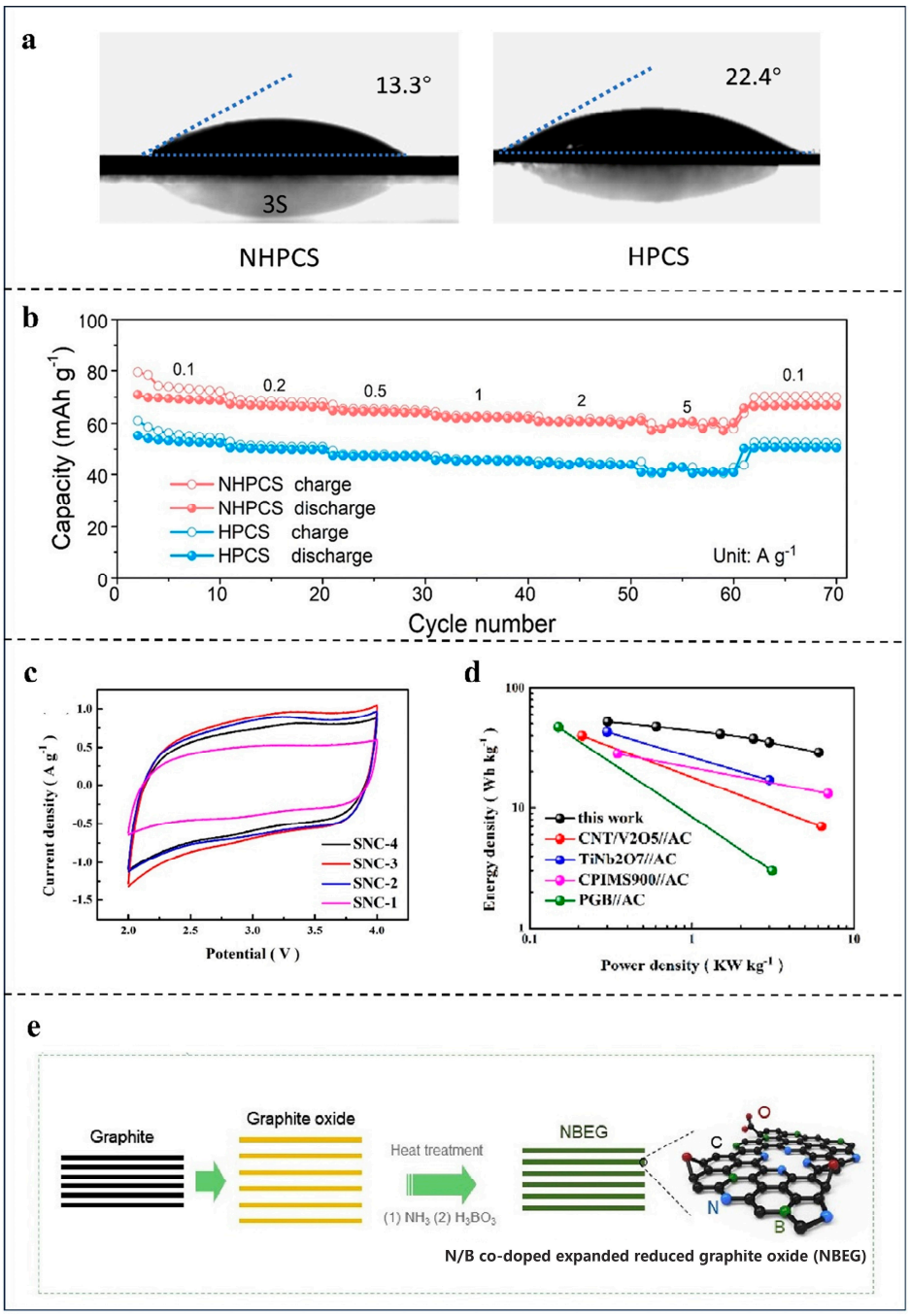



**Figure 4.** (**a**) The contact angles and (**b**) rate capabilities of the NHPCS and HPCS. Reproduced with permission from Ref. [107]. Copyright 2020, Springer Nature. (**c**) The CV curve of SNC1–4 samples at a scan rate of 10 mV $s^{-1}$. (**d**) A performance comparison of this LIC with other works. Reproduced with permission from Ref. [110]. Copyright 2023, Elsevier. (**e**) N/B co-doped expanded reduced graphite oxide (NBEG). Reproduced with permission from Ref. [119]. Copyright 2020, Elsevier.

**Table 2.** Estimated parameters from BET and EDS analysis.

| Material | $S_{BET}$ ($m^2$ $g^{-1}$) | $V_{tot}$ ($cm^3$ $g^{-1}$) | $V_{mic}$ ($cm^3$ $g^{-1}$) | $D_{DA}$ (nm) | Elemental Analysis (at%) | | | |
|---|---|---|---|---|---|---|---|---|
| | | | | | C1s | N1s | O1s | S2p |
| SNC-1 | 547 | 1.32 | 0.11 | 10.91 | 72.59 | 12.92 | 12.7 | 1.81 |
| SNC-2 | 619 | 1.32 | 0.03 | 9.68 | 71.03 | 11.91 | 10.52 | 6.55 |
| SNC-3 | 616 | 1.18 | 0.013 | 9.72 | 67.94 | 7.98 | 16.67 | 7.42 |
| SNC-4 | 514 | 1.43 | 0.017 | 11.58 | 56.15 | 5.7 | 24.62 | 13.54 |

$S_{BET}$: BET surface area. $V_{tot}$: total volume in pores. $V_{mic}$: micropore area. $D_{DA}$: desorption average pore diameter.

## 5. Element Doping for Dual-Carbon Electrodes

Carbon materials have broad prospects in the field of energy storage due to their large capacity and environmental friendliness [121]. The double-carbon alkali metal-ion capacitor (DC-AMIC), which utilizes carbon materials for both the positrode and negatrode, boasts the benefits of low cost, excellent stability, and adjustable surface compositions and structural morphology. For instance, dual-carbon sodium-ion capacitors (DC-SICs) select similar material systems for their negatrodes and positrodes, addressing the issues of capacity imbalance and kinetic mismatch between the two electrodes. The double-carbon system manifests in two primary forms: one where two distinct carbon materials with different properties serve as the negatrode and positrode, and another where the same carbon material is used for both. The former can fully utilize the advantages of different carbon materials, resulting in a significant improvement in both the capacity and power performance of DC-AMICs. The latter has a lower production cost, which is conducive to mass production and application, while the synergistic effect between the positrode and negatrode in the charging and discharging process will be enhanced.

### *5.1. Dual Electrodes Made of the Same Carbon Material*

#### 5.1.1. LIC

Research has demonstrated that atomic doping can significantly enhance the charge storage capacity of carbon materials. Li et al. [122] prepared a two-dimensional (2D) nitrogen-doped carbon nanosheet (NCN). The high-resolution transmission electron microscopy (HRTEM) image depicted in Figure 5a reveals the lattice stripe extension of the NCN (0.36 nm), providing evidence that the large interlayer distance of the carbon layer contributes to the high electrochemical conductivity of the NCN. This observation is closely associated with the abundant and uniformly distributed nitrogen within the NCN (Figure 5b). Furthermore, the porous structure of the carbon substrate (CNF) endows the NCN positrode with a high specific capacity, enabling excellent pseudo-capacitance storage dynamics even at high current rates. Using an NCN as the negatrode and positrode of the LIC not only reduces the cost but also effectively alleviates the dynamic imbalance, improving the electrochemical performance of the capacitor. The dual-carbon NCN//NCN LIC system can provide a high specific energy of 167 Wh $kg^{-1}$ at a specific power of 240 W $kg^{-1}$. Moreover, it exhibits good cycling stability (capacity retention of 85.6% for 9000 cycles at 1 A $g^{-1}$).

Jiang and colleagues have developed coal-based nitrogen-doped porous carbon materials (CNPCs) that feature a folded carbon nanosheet structure [123]. The use of g-C3N4 as both a templating agent and a nitrogen source plays a pivotal role in determining the pore size and nitrogen content of CNPCs, which in turn significantly impacts the electrochemical performance of these materials. In Figure 5c,d, the optimized CNPCs (CTK-1.0) display good pore regulation, high conductivity, and a large specific surface area. Scanning transmission electron microscopy (STEM) and energy-dispersive X-ray spectroscopy (EDS) analyses of CTK-1.0 confirm the uniform distribution of carbon and nitrogen ele-

ments within the CNPCs, signifying the successful doping with heteroatomic nitrogen (Figure 5e–g). The nitrogen-doped structures, specifically pyridinic N and pyrrolic N, offer additional active sites for pseudo-capacitance and ion adsorption, thereby enhancing the fast-charging capabilities of the materials. Moreover, ammonium N facilitates electron transfer within the carbon lattice [124], which enhances the capacity of dual-carbon lithium-ion capacitors (DC-LICs). The constructed CTK-1.0//CTK-1.0 LIC achieves a balanced capacity and kinetic balance, with a maximum specific energy of 137.6 Wh $kg^{-1}$ and a long lifetime of 3000 cycles.

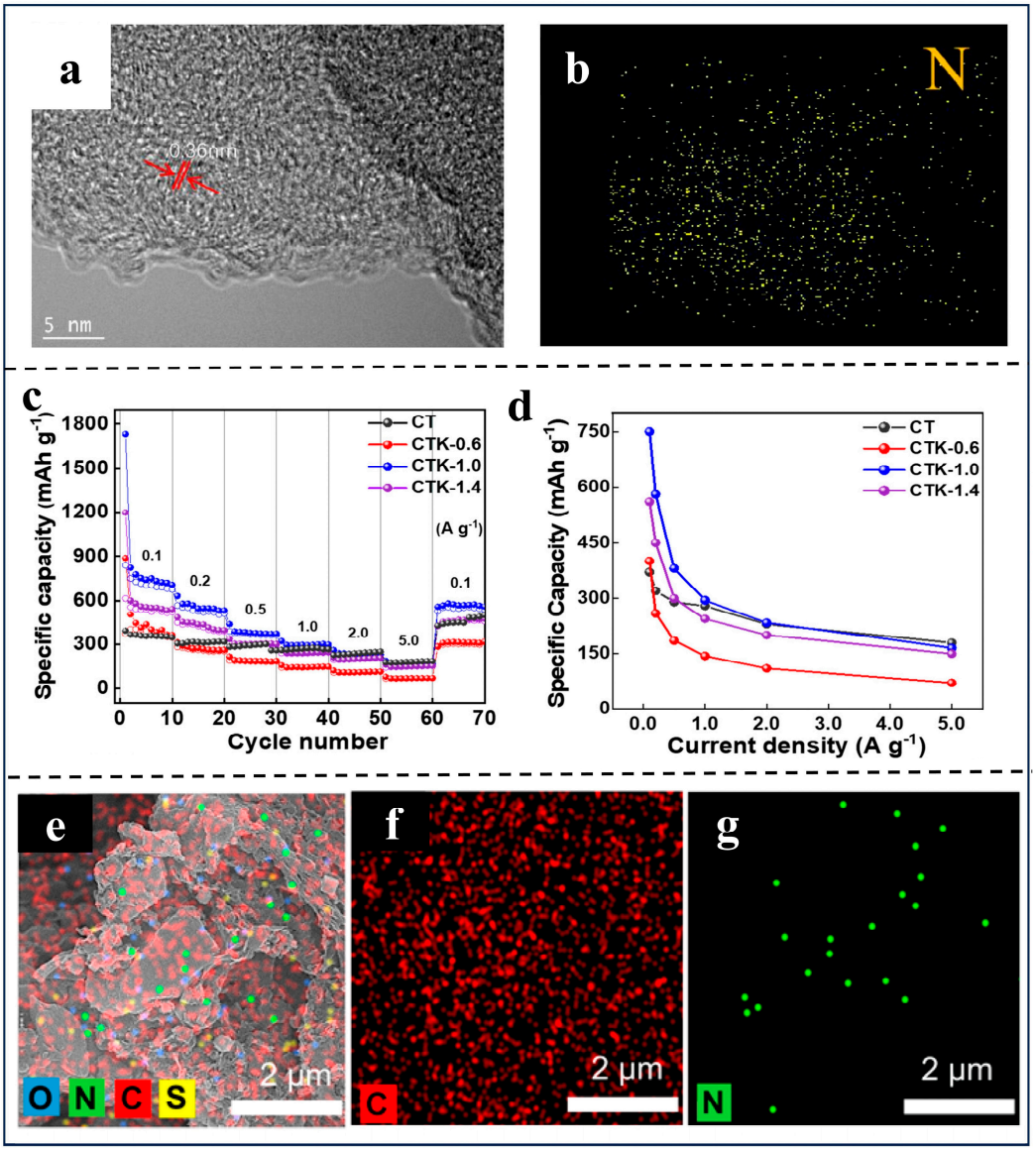



**Figure 5.** (**a**) HRTEM pictures of the NCN. TEM images (**b**) of the corresponding EDS elemental analysis of the NCN. Reproduced with permission from Ref. [122]. Copyright 2022, Elsevier. (**c**) The rate performance and (**d**) specific capacities at different current densities of CNPCs with different g-C additions. (**e**) STEM images of CTK-1.0 with the corresponding (**f**) C and (**g**) N elemental mappings. Reproduced with permission from Ref. [123]. Copyright 2023, Multidisciplinary Digital Publishing Institute.

Enhancing the low-temperature performance of LICs is a significant challenge in the energy storage industry. At low temperatures, the electrochemical reaction kinetics of capacitors slow down, adversely affecting ion transport and charge transfer, which in turn impedes the normal functioning of LICs. To address this problem, Xiao et al. [125] prepared

S-doped graphene nanocapsules (SGCs) as the negatrode and positrode of LICs. The storage mechanism of the prepared SGCs//SGCs LICs is shown in Figure 6a. As illustrated in Figure 6b, SGCs//SGCs LICs embody a capacity retention rate of more than 83% at −30 °C (10,000 cycles at 5 A $g^{-1}$ and 10 A $g^{-1}$), revealing excellent ultra-long cryogenic cycle performance. The superior performance of the SGC electrodes is attributed to their stable nanocapsule morphology, abundant pore volume, and S-doped structure. The presence of S contributes to a gradual decrease in the $Li^+$ migration rate under low-temperature test conditions. As shown in Figure 6c, the $Li^+$ diffusion coefficients of the SGC negatrode are significantly higher than those of the GC negatrode at −20 and −30 °C. Furthermore, by forming Li-S chemical bonds, the S-doped structure can also facilitate the storage of more $Li^+$ ions and generate larger pseudo-capacitance, enhancing the overall performance of the LICs under low-temperature conditions.

#### 5.1.2. SIC

Thangavel et al. [126] used graphene hollow nanospheres (GHNSs) doped with double heteroatoms (N and S) for the first time in the fabrication of symmetric DC-SICs. Initially, the NS-GHNSs exhibited a relatively low initial coulombic efficiency of only 36%, which was attributed to the formation of the solid electrolyte interphase (SEI) layer and irreversible reactions between carbon functional groups and sodium ions. However, the NS-GHNSs demonstrated stable performance in subsequent cycles (Figure 6d), achieving a coulombic efficiency of greater than 99% and maintaining a discharge capacity of 264 mAh $g^{-1}$. This improvement is credited to the presence of nitrogen and sulfur dopants, which enhance the electrical conductivity of the carbon substrate and help mitigate irreversible capacity loss during the initial cycling period. Additionally, there are a large number of heteroatom functional groups on the NS-GHNSs (Figure 6e,f), which have an irreplaceable advantage, for example, providing excellent wettability conducive to the transfer storage of $Na^+$ [127,128].

#### 5.1.3. KIC

Nitrogen-doped porous carbon nanosheets (NPCNs), serving a dual role, were crafted through a combination of carbonization and self-assembly techniques [129]. In Figure 6g, NPCN-900 shows a type IV curve, and the specific surface area is 1586 $m^2$ $g^{-1}$. This suggests that NPCN-900, with its ample pores and expansive surface area, offers swift diffusion channels and adsorption sites for potassium ions ($K^+$), thereby bolstering its capacitive performance. Similarly, the graphitic N in NPCN-900 can promote the formation of ordered structures, which gives NPCN-900 an ordered graphitic carbon structure [130]. Figure 6h illustrates the remarkable rate capability of NPCN-900, which substantiates its pre-eminent position among negatrode materials [124]. The superior performance can be attributed to three primary factors. The addition of nitrogen not only enriches the active sites on the carbon material, providing more adsorption sites for $K^+$, but also increases the spacing between the carbon layers, which reduces resistance and deformation during $K^+$ intercalation/decalcification. Likewise, the abundant pores of the porous carbon nanosheets improve the capacitance performance. The NPCN//NPCN KIC exhibits 128 Wh $kg^{-1}$ with high specific energy and excellent cycling stability (90.8% of the discharge capacity after 9000 cycles at 1.0 A $g^{-1}$). Notably, the capacity of the KIC shows a trend of decreasing and then increasing. It is shown that a large amount of hidden nitrogen is distributed inside the NPCN electrode, which is gradually activated during the long cycling process, thus releasing more active sites [131,132].

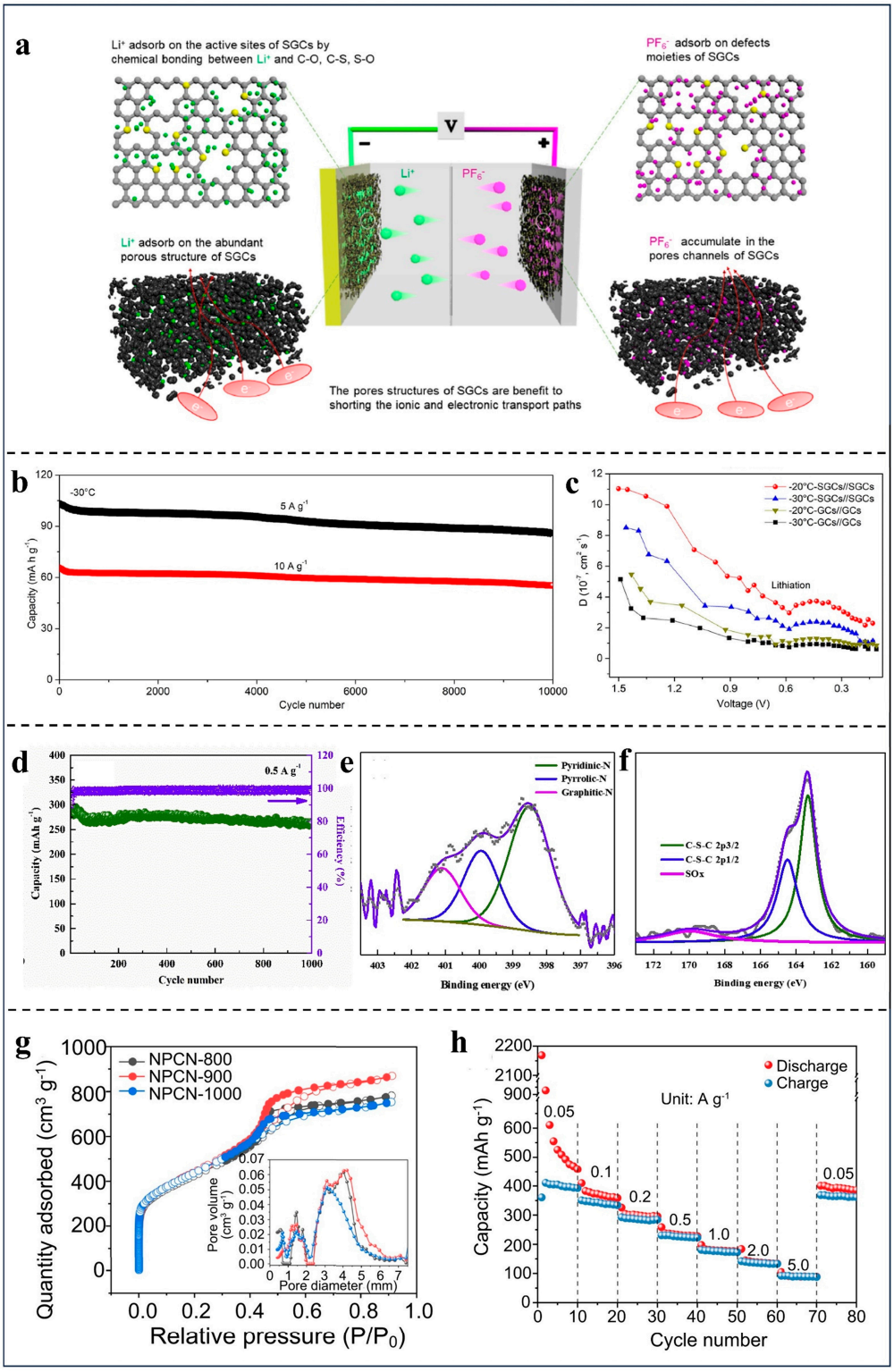



**Figure 6.** (**a**) A schematic illustration of the entire charge–discharge storage mechanisms of the as-prepared all-graphene symmetric SGCs//SGCs LIC. (**b**) The cycling performance of SGCs//SGCs after 10,000 cycles at −30 °C. (**c**) $Li^+$ diffusion coefficients of the SGC negatrode compared with GCs at low temperature. Reproduced with permission from Ref. [125]. Copyright 2022, Elsevier. (**d**) The anodic performance of NS-GHNSs, with cycling stability at 0.5 A $g^{-1}$. XPS survey spectra of NS-GHNSs, and high-resolution deconvoluted XPS spectra of (**e**) N1s, and (**f**) S2p. Reproduced with permission from Ref. [126]. Copyright 2019, Elsevier. (**g**) $N_2$ adsorption and desorption isotherms of NPCN-T (T = 800, 900, and 1000). (**h**) The rate capability of NPCN-900 as a negatrode for potassium-ion capacitors. Reproduced with permission from Ref. [129]. Copyright 2023, Elsevier.

### *5.2. Different Carbon Materials as Electrodes*

#### 5.2.1. LIC

In AMICs, the selection of negatrode materials with ample layer spacing and rapid kinetics is essential to facilitate the swift embedding/removal of $M^+$ [133,134]. For the positrode materials, in order to have an outstanding capacitive capacity, abundant active sites and a large specific surface area are necessary [135–137].

Gao et al. [138] synthesized phosphorus-doped activated carbon (PAC-6) by carbonation. Figure 7a shows the manufacturing process of PAC, and the schematic diagram of PHC-4//PAC-6 LIC is shown in Figure 7b. The elemental mapping is shown in Figure 7c, which indicates that P derived from phytic acid (PA) is uniformly doped throughout PAC-6. A higher P content (3.57%) creates active sites for a redox reaction with PAC-6, thus enhancing the capacity of the sample. As a result, the specific capacitance of PAC-6 reaches 147.1 F $g^{-1}$ at 0.05 A $g^{-1}$ with excellent rate capability (90% capacitance retention after 5000 cycles at 1.6 A $g^{-1}$). Due to the appropriate PA content, the high specific surface area (SSA) and ideal power spectral density (PSD) characteristics of PAC-6 contribute to its superior areal capacitance. The assembled LIC shows excellent energy power characteristics (maximum 122 Wh k $g^{-1}$, 9775 W k $g^{-1}$) and operating life.

The electrode kinetics of the negatrode can be significantly constrained by the low conductivity of the electrode material. Fortunately, researchers [139–141] found that S-doped carbon nanotubes (SCNTs) have high conductivity which can improve positrode and negatrode performance. This improvement is attributed to the ability of SCNTs to form a conductive network within the electrodes, thereby accelerating the ion transport rate. Zhao et al. [142] developed an integrated process suitable for sulfur doping in carbon materials, which led to the preparation of sulfur-doped porous carbon (SPC) and sulfur-doped carbon nanotubes (SCNTs). Due to sulfur doping, SPC exhibits an increased energy storage capacity and accelerated electrode kinetics. Then, $Li^+$ enters the SPC structure by adsorbing on S-containing active sites and inserts into interlayers/pores. The unique hydrophilicity and conductivity of SCNTs enable the construction of a uniformly distributed three-dimensional conductive network within the electrode, significantly enhancing the charge transfer rate and migration speed of $Li^+$ and $PF_6^-$ during the charging/discharging processes. The constructed AC-SCNTs//SPC-SCNT LIC possesses excellent electrochemical performance (Figure 7d), displaying a specific energy of 169 Wh $kg^{-1}$, excellent specific power of 1022 W $kg^{-1}$ at 136 Wh $kg^{-1}$.

#### 5.2.2. SIC

For DC-SIC, doping with heteroatom layers and constructing porous structures are two effective strategies that can significantly enhance the kinetic performance of carbon materials [91,143].

An NHPC-800//NHPAC SIC device was constructed by Zou et al. [144] using nitrogen-doped hierarchical porous carbon (NHPC) as the negatrode and nitrogen-doped hierarchical porous activated carbon (NHPAC) as the positrode. By virtue of the appropriate layer spacing (maximum at 0.42 nm) brought about by N doping and the hierarchical pores. This SIC has excellent specific energy (115 Wh $kg^{-1}$ at 200 W $kg^{-1}$) and a long lifecycle. Figure 7e demonstrates that the NHPC-800 electrode has the initial charge/discharge capacities of 392.4 mAh $g^{-1}$/ 536.3 mAh $g^{-1}$, respectively, with an ICE of 73.2%. Upon activation of NHPC to form NHPAC, both the porosity and specific surface area are enhanced, which is beneficial for the swift adsorption and desorption of anions ($ClO_4^-$) on the surface. Figure 7f shows the rate performance of the NHPAC electrode at various current densities. The specific capacity of the NHPAC electrode at 0.1 A $g^{-1}$ is 110 mAh $g^{-1}$, which is much higher than that of commercial activated carbon [145].

While the porous structure of electrode materials is indeed critical for $Na^+$ storage, pore sizes that are not appropriately tailored can adversely affect the performance of the electrodes.

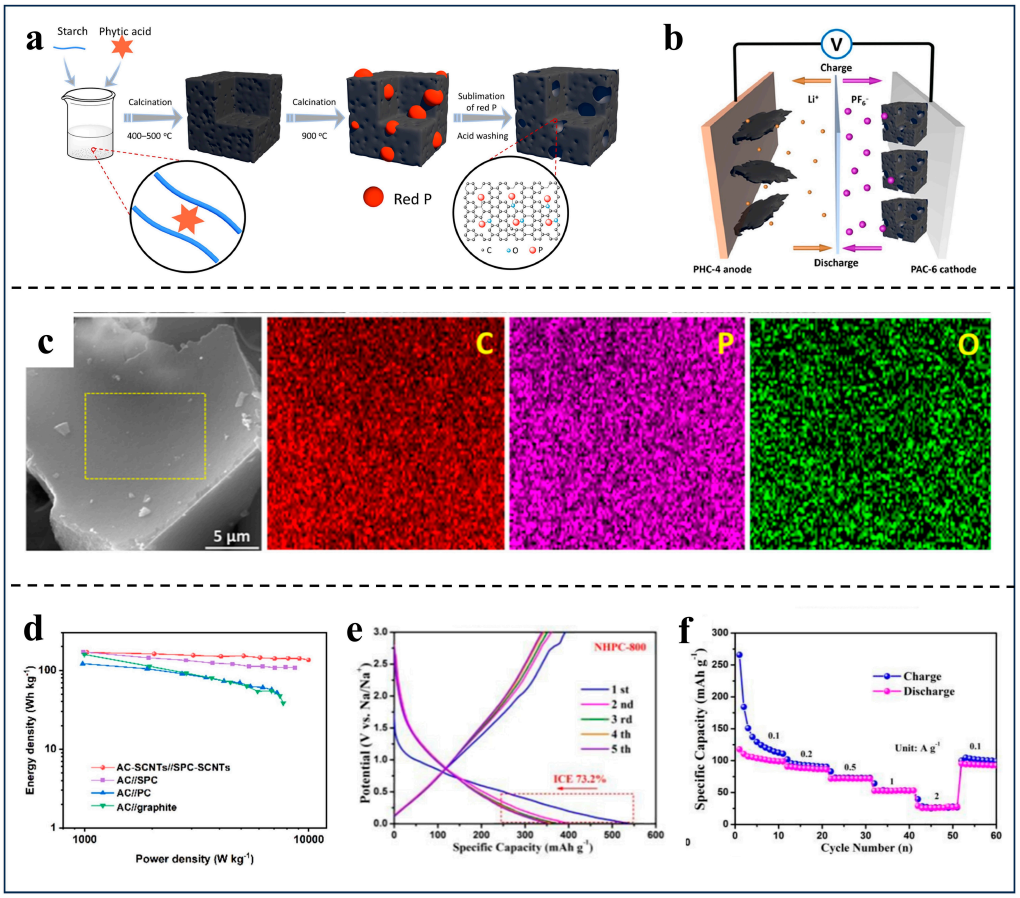



**Figure 7.** (**a**) Fabrication process for PACs. (**b**) Schematic of fabricated PHC-4//PAC-6 LIC. (**c**) SEM image of PAC-6 and corresponding elemental mapping images. Reproduced with permission from Ref. [138]. Copyright 2021, Elsevier. (**d**) Ragone diagram of assembled two-carbon AC-SCNT//SPC-SCNT LIC. Reproduced with permission from Ref. [142]. Copyright 2022, Elsevier. (**e**) GCD profiles of NHPC-800. (**f**) Rate capability of NHPAC positrode. Reproduced with permission from Ref. [144]. Copyright 2019, The Royal Society of Chemistry.

Wang et al. [146] doped hard carbon (HC) with N/S to enhance SIC performance and specific capacity. The structure of HC bent graphite was tuned by adding thiophene S, which has a characteristic heterocyclic structure, reducing the degree of graphitization and improving the wettability. Introducing more defects and edges during the carbonization process activates the electrochemical potential of the carbon, thereby boosting its electrical conductivity. Furthermore, the incorporation of nitrogen in the form of pyridinic N increases pseudo-capacitance and the capacity of the material. NS-pHC-1.348 (N and S co-doped porous hard carbon with 1.348 g $MgCl_2$ precursor) was prepared to provide reversible capacity, increased rate performance, and excellent cycling stability, which balances the electrochemical kinetics of the positrode and negatrode within the SIC. The NS-pHC-1.348//NPC SIC shows excellent specific power, reaching 92.03 kW $kg^{-1}$ at 5.98 Wh $kg^{-1}$.

### 5.2.3. KIC

For KIC, it is important to enhance the $K^+$ storage capacity to construct a porous carbonaceous negatrode with reasonable-sized defects and abundant active sites.

Liu and colleagues [147] expanded microporous defects while increasing the number of chemisorbed sites, and finally synthesized phosphorus–nitrogen double-doped foamy porous carbon (PN-FPC). The formation process of the PN-FPC material is shown in Figure 8a. P/N double doping constructs a defect-rich structure in PN-FPC, facilitating the reversible adsorption/desorption behaviors of $K^+$. The rich mesoporous structure and fine size of

PN-FPC forms an inter-connection structure between the carbon bubbles (Figure 8b,c), which allows $K^+$ to move fast. As the scanning rate increases, the capacitance contribution of the PN-FPC electrode gradually increases, demonstrating that the synergy between P/N co-doping and the carbon matrix results in excellent enhancement in reaction kinetics. Meanwhile, by observing the P-C (133.5 eV) and P-O (132.5 eV) peaks in the P 2p spectra (Figure 8g), it is demonstrated that the P-O functional group could improve the wettability of PN-FPC, shortening the charge transfer process of $K^+$ [148]. Figure 8d illustrates that PN-FAPC, used as the positrode, maintains a reversible capacity of 110.2 mAh $g^{-1}$ at a high rate of 5 A $g^{-1}$, showcasing its excellent structural stability. It exhibits a long-term lifecycle of 86.3% capacity retention over 1000 charge/discharge cycles (Figure 8e). The PN-FPC//PN-FAPC KIC shows ultra-high specific energy (155.6 Wh $kg^{-1}$), specific power (17,000 W $kg^{-1}$), and an ultra-long lifetime (90.9% capacity retention after 10,000 cycles), as shown in Figure 8f.

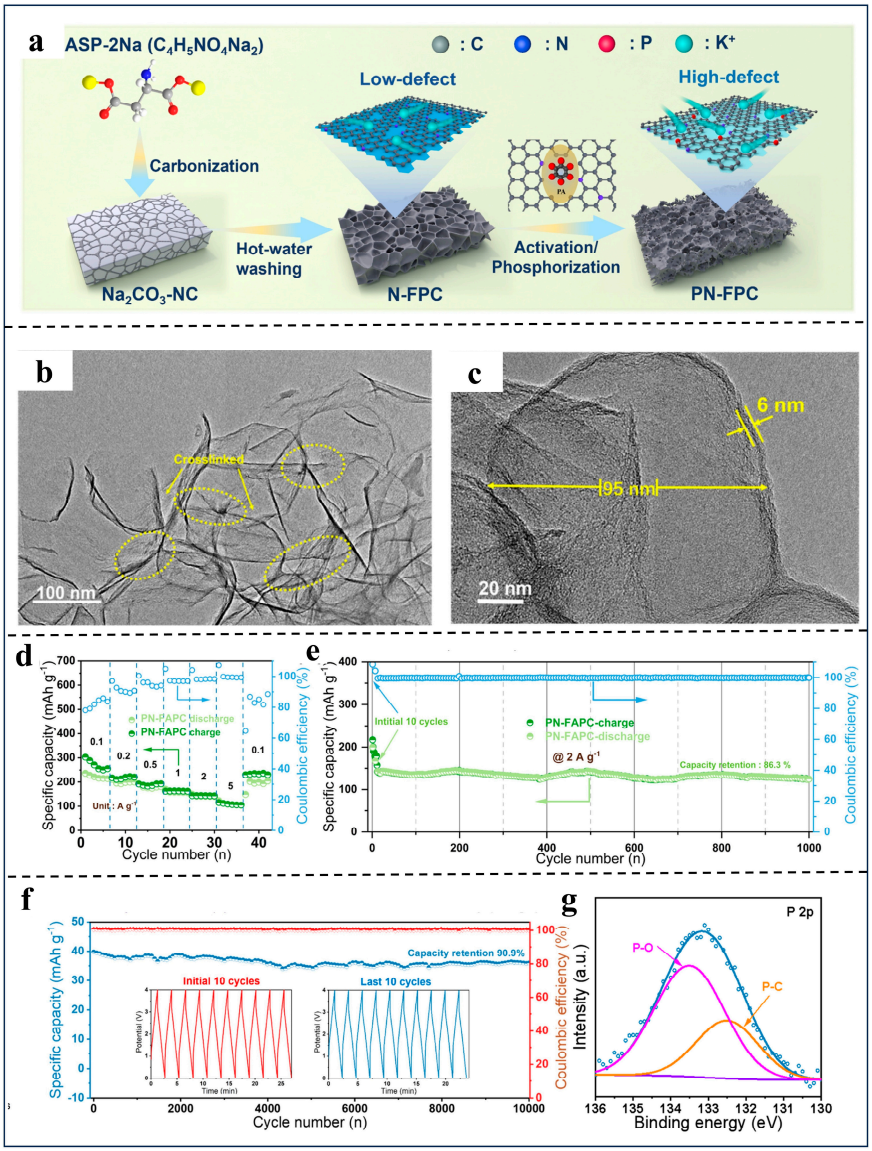



**Figure 8.** (**a**) A schematic illustration of the formation process of PN-FPC. (**b**,**c**) TEM images of PN-FPC. Half-cell performance of the PN-FAPC electrode tested between 1.5 and 4.2 V vs. K. (**d**) The rate performance and (**e**) lifecycle performance of the PN-FPC positrode (initial 10 cycles worked at 0.1 A $g^{-1}$). (**f**) The long-term cycling performance of the PN-FPC//PN-FAPC KIC at 2 A $g^{-1}$ in full-cell configuration. (The inset shows GCD curves for the first 10 cycles and the last 10 cycles.) (**g**) The high-resolution XPS spectrum of PN-FPC of P 2p and its deconvolution. Reproduced with permission from Ref. [147]. Copyright 2024, Elsevier.

## 6. Discussion and Conclusions

This review has systematically summarized the recent advancements in doped carbon materials for alkali metal-ion capacitors (AMICs) with M = Li, Na, and K, as well as the mechanisms by which doping atoms such as nitrogen (N), sulfur (S), phosphorus (P), and boron (B) influence the properties of AMICs. Table 3 reports a summary of the synthesis methods and electrochemical performance of heteroatom co-doped carbon-based materials. By employing diverse synthesis strategies and combining unique precursors with dopants, carbon substrates have been crafted into a variety of electrode materials with superior characteristics. These include single-element-doped carbons (N-, S-, P-, and B-doped) and materials with double-element doping. While there has been a surge in research on heteroatom doping in carbon materials in recent years, leading to significant progress, numerous challenges remain in the practical application of these doped carbon materials as electrode materials for AMICs.

**Table 3.** A summary of the synthesis methods and electrochemical performance of heteroatom co-doped carbon-based materials.

| Materials | Synthesis Method | Heteroatom Content% | Electrochemical System | Working Window | Cycling Data [a] | Rate Capacity [b] | Ref. |
|---|---|---|---|---|---|---|---|
| LGNC (4:1) | The denitrification and carbonization | N: 23.1at% | LIB | 0.01–3.0 V | 1499/100 | 1556/1 | [45] |
| C-N-30-8h | molten salt method | N: 1–2at% | SIB | 0.01–3.0 V | 179/500 | 179/1 | [46] |
| $As_8Mg$ | Template-assisted synthesis | N: 17wt.% | SIC | 0.01–2.0 V | 192/600 | 159/1 | [59] |
| INC | calcination | N: 5.63wt.% | LIC | 0.01–3.0 V | 280/3000 | 316/1 | [60] |
| CS-700m | Ball milling process | S: 19.8wt.% | SIC | 0.01–3.0 V | 370/200 | 280/1 | [68] |
| PHC-4 | Esterification and carbonation reactions | P: 3.44at% | LIC | 0.01–3.0 V | 84.7%/5000 | 770.4/0.1 | [75] |
| BGNS | Thermal reduction | B: 3.01wt.% | LIC | 1.9–4.0 V | 404/1000 | 800/0.1 | [85] |
| NSC | Molten salt method and carbonization | N: 5.6wt.%<br>S: 2.3wt.% | LIC | 2.0–4.5 V | 91.5%/10,000 | 81/1 | [92] |
| NHPCS | Template-assisted methods | N: 3.65at% | | 2.0–4.3 V | 88.7%/10,000 | 74/0.1 | [107] |
| NBEG | Calcination (purify by heating) | | SIC | 1.5–4.2 V | | 328/0.5 | [119] |
| SNC-3 | Template-assisted methods | S: 7.42at%<br>N: 7.98at% | LIC | 2.0–4.0 V | 90%/5000 | 78/0.1 | [110] |
| NCN | Template-assisted methods | N: 7.98at% | LIC | Negatrode: 0.01–3.0 V<br>Positrode: 0.5–4.3 V | Negatrode: 620/1000<br>Positrode: 110/1000 | Negatrode: 1129/0.1<br>Positrode: 110/1.0 | [122] |
| CTK-1.0 | Carbonization in argon atmosphere | N: 3.03at% | LIC | 0.01–3.0 V | 97%/800 | 750/0.1 | [123] |
| SGCs | Chemical Vapor Deposition (CVD) methods | S: 3.3at% | LIC | Negatrode: 0–1.5V<br>Positrode: 1.5–4.5V | Negatrode: 98.8%/10,000<br>Positrode: 89.1%/10,000 | Negatrode: 336/0.1<br>Positrode: 1668/0.1 | [125] |
| NS-GHNS | | N: 3.34wt.%<br>S: 1.82wt.% | SIC | Negatrode: 0.01–3.0 V<br>Positrode: 2.5–4.2 V | Negatrode: 86%/10,000<br>Positrode: 92%/10,000 | Negatrode: 630/0.1<br>Positrode: 52/0.2 | [126] |
| NPCNs | Carbonation Self-Assembly method | N: 6.60wt.% | PIC | 0.01–3.0 V<br>0.01–4.0 V | | 176/1.0<br>82.8/0.1 | [129] |
| PAC-6 | Esterification and carbonation reactions | P: 3.57wt.% | LIC | 0.01–3.0 V | 90%/10,000 | 147.1/0.05 | [138] |
| SPC-SCNTs | Template-assisted methods | S: 17.3wt.% | LIC | 0.01–1.5 V | | 348/0.5 | [142] |
| NHPC-800 | Pyrolysis | N: 10.4wt.% | SIC | 0.01–3.0 V | | 392.4/0.1 | [144] |
| AC-SCNTs | Activation method | N: 2.1wt.% | SIC | 2.0–4.5 V | | 110/0.1 | [144] |
| NS-pHC-1.348 | Carbonization and pickling | S: 7.77wt.% | SIC | 0.01–2.5 V | | 383.9/0.05 | [146] |
| PN-FPC | One-pot activation and phosphatization | N: 7.2wt.%<br>P: 1.9wt.% | PIC | 0.01–3.0 V | 88.9%/1000 | 201.1/5 | [147] |
| PN-FAPC | Carbonation | N: 5.1wt.% | PIC | 1.5–4.2 V | 86.3%/1000 | 110.2/5 | [147] |

[a] The cycling data are summarized as capacity (mAh $g^{-1}$)/corresponding cycle numbers. [b] The rate capacity is summarized as capacity (mAh $g^{-1}$) at a specific current (A $g^{-1}$).

(1) The incorporation of various doping elements can enhance distinct chemical properties of carbon materials. For instance, the concentration of B doping is pivotal to altering

the electronic mobility within B-containing carbon and the mobility of metal ions. Similarly, different forms of nitrogen doping, such as pyrrolic N and pyridinic N, exert specific influences on the chemical properties of the carbon material. In the case of double-element-doped carbon, selecting the appropriate elements and the optimal doping ratio is crucial for achieving a better balance between the negatrode and positrode. It is important to note that while doping elements are effective in enhancing the properties of carbon materials, suitable doping levels and precise doping locations require extensive and in-depth investigation.

(2) Carbon materials from different groups possess distinct structural features, and these variations can markedly influence how doping elements affect their properties. For instance, the two-dimensional planar structure of graphene endows it with a high specific surface area and superior electrical conductivity. N doping can further enhance its electron transport capacity, thereby improving the overall electrical conductivity of the material. This makes graphene particularly suitable for applications that necessitate swift charge transfer. On the other hand, activated carbon, known for its rich pore structure, experiences an increase in surface active sites and improved ion adsorption capacity when doped with elemental phosphorus. This enhancement bolsters its capacitive performance, making it an effective electrode material. At present, due to the limitations in our research understanding, further exploration and investigation are needed to uncover how the structure of carbon materials can enhance specific chemical properties. Advanced characterization techniques and theoretical calculations can provide a deeper understanding of the interaction mechanisms between doping elements and the structure of carbon substrates.

(3) Doped carbon materials with a high specific surface area indeed offer a greater number of active sites, which enhances the adsorption and storage capabilities for $M^+$. However, an excessively large specific surface area can lead to excessive consumption of the electrolyte in the initial cycle. The numerous active sites can interact strongly with the electrolyte, leading to the formation of a thick solid electrolyte interphase (SEI) film on the electrode surface. This SEI film formation consumes a significant amount of $Li^+$, causing substantial energy loss for the electrochemical device. Additionally, the overconsumption of the electrolyte results in a large amount of $Li^+$ being irreversibly intercalated into the electrode material during the first charge/discharge process, thereby reducing the initial coulombic efficiency (ICE). Therefore, designing doped carbon with an appropriate specific surface area is essential to strike a balance between achieving high capacity and maintaining high ICE.

In summary, the key to the design of doped carbon materials with excellent performance lies in mastering the type of doping atoms, the choice of concentration, and the design of a suitable specific surface area. At present, the practical application of doped carbon materials in AMICs has shown some potential but is still immature. Future research should continue to explore optimization strategies of doped carbon materials to overcome the current challenges and to promote the overall performance of AMICs for wider and more efficient applications in the field of energy storage.

**Author Contributions:** Conceptualization, K.Z.; methodology, T.Y. and X.H.; software, X.Y.; validation, X.H.; formal analysis, Y.G. and T.N.; investigation, Y.G. and L.Q.; resources, K.Z. and L.T.; data curation, T.Y.; writing—original draft preparation, T.Y. and Y.G.; writing—review and editing, X.H.; visualization, T.Y.; supervision, K.Z. and X.H.; project administration, L.L.; funding acquisition, K.Z. and L.L. All authors have read and agreed to the published version of the manuscript.

**Funding:** This work was supported by the National Natural Science Foundation of China (52374299, 52304320, and 52204306), the Outstanding Youth Foundation of Hunan Province (2023JJ10044), the

Scientific Research Fund of Hunan Provincial Department of Education (24B0295), the Natural Science Foundation of Hunan Province (2023JJ40014), and the Innovation and Entrepreneurship Training Program of Hunan Province (S202310536164).

**Conflicts of Interest:** The author declares no conflicts of interest.

## References

1. Liu, Z.; Wang, J.; Lu, B. Plum pudding model inspired $KVPO_4F$@3DC as high-voltage and hyperstable cathode for potassium ion batteries. *Sci. Bull.* **2020**, *65*, 1242–1251. [CrossRef]
2. Zou, K.; Jiang, M.; Ning, T.; Tan, L.; Zheng, J.; Wang, J.; Ji, X.; Li, L. Thermodynamics-directed bulk/grain-boundary engineering for superior electrochemical durability of Ni-rich cathode. *J. Energy Chem.* **2024**, *97*, 321–331. [CrossRef]
3. Zhang, X.; Wang, L.; Liu, W.; Li, C.; Wang, K.; Ma, Y. Recent advances in MXenes for lithium-ion capacitors. *ACS Omega* **2020**, *5*, 75–82. [CrossRef] [PubMed]
4. Dai, M.; Zhao, D.; Wu, X. Research progress on transition metal oxide based electrode materials for asymmetric hybrid capacitors. *Chin. Chem. Lett.* **2020**, *31*, 2177–2188. [CrossRef]
5. Amatucci, G.G.; Badway, F.; Pasquier, D.A.; Zheng, T. An asymmetric hybrid nonaqueous energy storage cell. *J. Electrochem. Soc.* **2001**, *148*, A930–A939. [CrossRef]
6. Soltani, M.; Beheshti, S.H. A comprehensive review of lithium ion capacitor: Development, modelling, thermal management and applications. *J. Energy Storage* **2021**, *34*, 102019. [CrossRef]
7. Nagamuthu, S.; Zhang, Y.; Xu, Y.; Sun, J.; Zhang, Y.; Zaman, F.; Denis, D.; Hou, L.; Yuan, C. Non-lithium-based metal ion capacitors: Recent advances and perspectives. *J. Mater. Chem. A* **2022**, *10*, 357–378. [CrossRef]
8. Liu, W.; Zhang, X.; Li, C.; Wang, K.; Sun, X.; Ma, Y. Carbon-coated $Li_3VO_4$ with optimized structure as high capacity anode material for lithium-ion capacitors. *Chin. Chem. Lett.* **2020**, *31*, 2225–2229. [CrossRef]
9. Cao, L.; Li, H.; Liu, X.; Liu, S.; Zhang, L.; Xu, W.; Yang, H.; Hou, H.; He, S.; Zhao, Y.; et al. Nitrogen, sulfur co-doped hierarchical carbon encapsulated in graphene with "sphere-in-layer" interconnection for high-performance supercapacitor. *J. Colloid Interface Sci.* **2021**, *599*, 443–452. [CrossRef]
10. Ma, X.; Gao, D. High capacitive storage performance of sulfur and nitrogen codoped mesoporous graphene. *ChemSusChem* **2018**, *11*, 1048–1055. [CrossRef] [PubMed]
11. Jiang, M.; Wang, P.; Chen, Q.; Zhang, Y.; Wu, Q.; Tan, L.; Ning, T.; Li, L.; Zou, K. Enabling the Nb/Ti co-doping strategy for improving structure stability and rate capability of Ni-rich cathode. *Chin. Chem. Lett.* **2024**, *35*, 110040. [CrossRef]
12. Wang, B.; Gao, X.; Xu, L.; Zou, K.; Cai, P.; Deng, X.; Yang, L.; Hou, H.; Zou, G.; Ji, X. Advanced carbon materials for sodium-ion capacitors. *Batter. Supercaps* **2021**, *4*, 538–553. [CrossRef]
13. Zhou, J.; Hu, H.; Li, H.; Chen, Z.; Yuan, C.; He, X. Advanced carbon-based materials for Na, K, and Zn ion hybrid capacitors. *Rare Met.* **2023**, *42*, 719–739. [CrossRef]
14. Li, L.; Chen, Q.; Jiang, M.; Ning, T.; Tan, L.; Zhang, X.; Zheng, J.; Wang, J.; Wu, Q.; Ji, X.; et al. Uncovering mechanism behind tungsten bulk/grain-boundary modification of Ni-rich cathode. *Energy Storage Mater.* **2025**, *75*, 104016. [CrossRef]
15. Peng, Y.; Bai, Y.; Liu, C.; Cao, S.; Kong, Q.; Pang, H. Applications of metal-organic framework-derived N, P, S doped materials in electrochemical energy conversion and storage. *Coord. Chem. Rev.* **2022**, *466*, 214602. [CrossRef]
16. Zhang, J.; Fang, J.; Han, J.; Yan, T.; Shi, L.; Zhang, D. N, P, S co-doped hollow carbon polyhedra derived from MOF-based core-shell nanocomposites for capacitive deionization. *J. Mater. Chem. A* **2018**, *6*, 15245–15252. [CrossRef]
17. Zou, K.; Xie, S.; Jiang, M.; Wang, P.; Ning, T.; Tan, L.; Li, H.; Zhou, Y.; Wang, W.; Li, L. Insights into the precursor specific surface area for engineering Co-free Ni-rich cathodes with tailorable properties. *Chem. Eng. J.* **2024**, *483*, 149189. [CrossRef]
18. Feng, X.; Bai, Y.; Liu, M.; Li, Y.; Yang, H.; Wang, X.; Wu, C. Untangling the respective effects of heteroatom-doped carbon materials in batteries, supercapacitors and the ORR to design high performance materials. *Energy Environ. Sci.* **2021**, *14*, 2036–2089. [CrossRef]
19. Shao, T.; Liu, C.; Deng, W.; Li, C.; Wang, X.; Xue, M.; Li, R. Recent research on strategies to improve ion conduction in alkali metal-ion batteries. *Batter. Supercaps* **2019**, *2*, 403–427. [CrossRef]
20. Chen, Z. Supercapacitor and supercapattery as emerging electrochemical energy stores. *Int. Mater. Rev.* **2017**, *62*, 173–202. [CrossRef]
21. Shao, H.; Wu, Y.; Lin, Z.; Taberna, P.; Simon, P. Nanoporous carbon for electrochemical capacitive energy storage. *Chem. Soc. Rev.* **2020**, *49*, 3005–3039. [CrossRef] [PubMed]
22. Mirzaeian, M.; Abbas, Q.; Gibson, D.; Mazur, M. Effect of nitrogen doping on the electrochemical performance of resorcinol-formaldehyde based carbon aerogels as electrode material for supercapacitor applications. *Energy* **2019**, *173*, 809–819. [CrossRef]
23. Rudra, S.; Seo, H.; Sarker, S.; Kim, D. Supercapatteries as hybrid electrochemical energy storage devices: Current status and future prospect. *Molecules* **2024**, *29*, 243. [CrossRef] [PubMed]

24. Sun, Y.; Wang, H.; Wei, W.; Zheng, Y.; Tao, L.; Wang, Y.; Huang, M.; Shi, J.; Shi, Z.; Mitlin, D. Sulfur-rich graphene nanoboxes with ultra-high potassiation capacity at fast charge: Storage mechanisms and device performance. *ACS Nano* **2021**, *15*, 1652–1665. [CrossRef] [PubMed]
25. Zou, K.; Jiang, M.; Zhao, Z.; Xie, S.; Ning, T.; Tan, L.; Li, H.; Zhou, Y.; Wang, W.; Wu, X.; et al. Mechanistic insights into suppressing microcracks by regulating grain size of precursor for high-performance Ni-rich cathodes. *Chem. Eng. J.* **2023**, *476*, 146793. [CrossRef]
26. González, A.; Goikolea, E.; Barrena, J.A.; Mysyk, R. Review on supercapacitors: Technologies and materials. *Renew. Sustain. Energy Rev.* **2016**, *58*, 1189–1206. [CrossRef]
27. Wu, M.; Hu, X.; Zheng, W.; Chen, L.; Zhang, Q. Recent advances in porous carbon nanosheets for high-performance metal-ion capacitors. *Chem. Eng. J.* **2023**, *466*, 143077. [CrossRef]
28. Cao, B.; Li, X. Recent progress on carbon-based anode materials for Na-ion batteries. *Acta Phys.-Chim. Sin.* **2020**, *36*, 1905003. [CrossRef]
29. Zhao, C.; Wei, Y.; Pan, Y.; Chen, C. A novel strategy for capacity judgement of hard carbon in sodium-ion batteries: Ensuring the consistency of the available anode capacity between half-cell and full-cell. *Solid State Ion.* **2024**, *412*, 116586. [CrossRef]
30. Han, P.; Xu, G.; Han, X.; Zhao, J.; Zhou, X.; Cui, G. Lithium ion capacitors in organic electrolyte system: Scientific problems, material development, and key technologies. *Adv. Energy Mater.* **2018**, *8*, 1801243. [CrossRef]
31. Li, B.; Zhen, J.; Zhang, H.; Jin, L.; Yang, D.; Lv, H.; Shen, C.; Shellikeri, A.; Zheng, Y.; Gong, R.; et al. Electrode materials, electrolytes, and challenges in nonaqueous lithium-ion capacitors. *Adv. Mater.* **2018**, *30*, 1705670. [CrossRef]
32. Wei, Q.; Liu, J.; Feng, W.; Sheng, J.; Tian, X.; He, L.; An, Q.; Mai, L. Hydrated vanadium pentoxide with superior sodium storage capacity. *J. Mater. Chem. A* **2015**, *3*, 8070–8075. [CrossRef]
33. Wang, H.; Zhu, C.; Chao, D.; Yan, Q.; Fan, H. Nonaqueous hybrid lithium-ion and sodium-ion capacitors. *Adv. Mater.* **2017**, *29*, 1702093. [CrossRef] [PubMed]
34. Shi, R.; Han, C.; Li, H.; Xu, L.; Zhang, T.; Li, J.; Lin, Z.; Wong, C.; Kang, F.; Li, B. NaCl-templated synthesis of hierarchical porous carbon with extremely large specific surface area and improved graphitization degree for high energy density lithium ion capacitors. *J. Mater. Chem. A* **2018**, *6*, 17057–17066. [CrossRef]
35. Li, N.; Du, X.; Shi, J.; Zhang, X.; Fan, W.; Wang, J.; Zhao, S.; Liu, Y.; Xu, W.; Li, M.; et al. Graphene@hierarchical meso-/microporous carbon for ultrahigh energy density lithium-ion capacitors. *Electrochim. Acta* **2018**, *281*, 459–465. [CrossRef]
36. Ma, H.; Geng, H.; Yao, B.; Wu, M.; Li, C.; Zhang, M.; Chi, F.; Qu, L. Highly ordered graphene solid: An efficient platform for capacitive sodium-ion storage with ultrahigh volumetric capacity and superior rate capability. *ACS Nano* **2019**, *13*, 9161–9170. [CrossRef]
37. Cao, Y.; Mao, S.; Li, M.; Chen, Y.; Wang, Y. Metal/porous carbon composites for heterogeneous catalysis: Old catalysts with improved performance promoted by N-doping. *ACS Catal.* **2017**, *7*, 8090–8112. [CrossRef]
38. Inagaki, M.; Toyoda, M.; Soneda, Y.; Morishita, T. Nitrogen-doped carbon materials. *Carbon* **2018**, *132*, 104–140. [CrossRef]
39. Du, J.; Liu, L.; Yu, Y.; Zhang, Y.; Lv, H.; Chen, A. N-doped ordered mesoporous carbon spheres derived by confined pyrolysis for high supercapacitor performance. *J. Mater. Sci. Technol.* **2019**, *35*, 2178–2186. [CrossRef]
40. Lv, Q.; Si, W.; He, J.; Sun, L.; Zhang, C.; Wang, N.; Yang, Z.; Li, X.; Wang, X.; Deng, W.; et al. Selectively nitrogen-doped carbon materials as superior metal-free catalysts for oxygen reduction. *Nat. Commun.* **2018**, *9*, 3376. [CrossRef]
41. Tan, H.; Tang, J.; Kim, J.; Kaneti, Y.; Kang, Y.; Sugahara, Y.; Yamauchi, Y. Rational design and construction of nanoporous iron- and nitrogen-doped carbon electrocatalysts for oxygen reduction reaction. *J. Mater. Chem. A* **2019**, *7*, 1380–1393. [CrossRef]
42. Wang, X.; Li, X.; Zhang, L.; Yoon, Y.; Weber, P.; Wang, H.; Guo, J.; Dai, H. N-doping of graphene through electrothermal reactions with ammonia. *Science* **2009**, *324*, 768–771. [CrossRef]
43. Paraknowitsch, P.; Thomas, A.; Antonietti, M. A detailed view on the polycondensation of ionic liquid monomers towards nitrogen doped carbon materials. *J. Mater. Chem.* **2010**, *20*, 6746–6758. [CrossRef]
44. Seredych, M.; Hulicova-Jurcakova, D.; Lu, G.; Bandosz, T. Surface functional groups of carbons and the effects of their chemical character, density and accessibility to ions on electrochemical performance. *Carbon* **2008**, *46*, 1475–1488. [CrossRef]
45. Tang, Y.; Chen, J.; Mao, Z.; Roth, C.; Wang, D. Highly N-doped carbon with low graphitic-N content as anode material for enhanced initial coulombic efficiency of lithium-ion batteries. *Carbon Energy* **2022**, *5*, e257. [CrossRef]
46. Zhao, J.; Song, Q.; Zhao, H.; Xie, H.; Ning, Z.; Yu, K. Molten salt splitting of $CO_2$ with $CaC_2$ and in-situ nitrogen doping for carbon anode of lithium/sodium-ion batteries. *J. Electroanal. Chem.* **2023**, *950*, 117845. [CrossRef]
47. Zhang, C.; Zhong, X.; Chen, P.; Sun, S.; Jiang, Y.; Yan, X. Facile synthesis of porous graphite by calcium carbide and nitrogen gas for lithium-ion batteries. *J. Energy Storage* **2023**, *66*, 107386. [CrossRef]
48. Sadezky, A.; Muckenhuber, H.; Grothe, H.; Niessner, R.; Pöschl, U. Raman microspectroscopy of soot and related carbonaceous materials: Spectral analysis and structural information. *Carbon* **2005**, *43*, 1731–1742. [CrossRef]
49. Rivera–Utrilla, J.; Ferro–García, M.A. Effect of carbon-oxygen and carbon-nitrogen surface complexes on the adsorption of cations by activated carbons. *Adsorpt. Sci. Technol.* **1986**, *3*, 293–302. [CrossRef]

50. Keegel, F.; Suruda, A.; Schwob, C. The catalytic properties of charcoal. III. A comparison of the oxidative properties of various charcoals. The effect of charcoal hydrosols on hydrogen peroxide and oxygen. *J. Am. Chem. Soc.* **1938**, *60*, 2483–2486. [CrossRef]
51. Stöhr, B.; Boehm, H.; Schlögl, R. Enhancement of the catalytic activity of activated carbons in oxidation reactions by thermal treatment with ammonia or hydrogen cyanide and observation of a superoxide species as a possible intermediate. *Carbon* **1991**, *29*, 707–720. [CrossRef]
52. Boehm, H. Catalytic properties of nitrogen-containing carbons. *Carbon Mater. Catal.* **2008**, *7*, 219–265. [CrossRef]
53. Fu, W.; Zhang, K.; Chen, M.; Zhang, M.; Shen, Z. One-pot synthesis of N-doped hierarchical porous carbon for high-performance aqueous capacitors in a wide pH range. *J. Power Sources* **2021**, *491*, 229587. [CrossRef]
54. Luo, X.; Yang, Q.; Dong, Y.; Huang, X.; Kong, D.; Wang, B.; Liu, H.; Xiao, Z.; Zhi, L. Maximizing pore and heteroatom utilization within N, P-co-doped polypyrrole-derived carbon nanotubes for high-performance supercapacitors. *J. Mater. Chem. A* **2020**, *8*, 17558–17567. [CrossRef]
55. Xu, Y.; Zhang, C.; Zhou, M.; Fu, Q.; Zhao, C.; Wu, M.; Lei, Y. Highly nitrogen doped carbon nanofibers with superior rate capability and cyclability for potassium ion batterie. *Nat. Commun.* **2018**, *9*, 1720. [CrossRef]
56. Chen, Z.; Zhao, S.; Zhou, Y.; Yu, C.; Zhong, W.; Yang, W. Nacre-like laminate nitrogen-doped porous carbon/carbon nanotubes/graphene composite for excellent comprehensive performance supercapacitors. *Nanoscale* **2018**, *10*, 15229–15237. [CrossRef]
57. Sanchez-Sanchez, A.; Izquierdo, M.; Mathieu, S.; González-Álvarez, J.; Celzard, A.; Fierro, V. Outstanding electrochemical performance of highly N- and O-doped carbons derived from pine tannin. *Green Chem.* **2017**, *19*, 2653–2665. [CrossRef]
58. Li, Z.; Cao, L.; Chen, W.; Huang, Z.; Liu, H. Mesh-like carbon nanosheets with high-level nitrogen doping for high-energy dual-carbon lithium-ion capacitors. *Small* **2019**, *15*, e1805173. [CrossRef] [PubMed]
59. Li, C.; Song, Z.; Liu, M.; Lepre, E.; Antonietti, M.; Zhu, J.; Liu, J.; Fu, Y.; López-Salas, N. Template-induced graphitic nanodomains in nitrogen-doped carbons enable high-performance sodium-ion capacitors. *Energy Environ. Mater.* **2024**, *7*, e12695. [CrossRef]
60. Chen, J.; Zhu, Y.; Luo, D.; Ma, G.; Zhao, Y.; Liu, B.; Yang, B.; Li, Y. Interconnected N-doped carbon network as high-performance anode material for superior lithium ion hybrid capacitor. *Mater. Today Commun.* **2023**, *34*, 105142. [CrossRef]
61. Ma, C.; Shao, X.; Cao, D. Nitrogen-doped graphene nanosheets as anode materials for lithium ion batteries: A first-principles study. *J. Mater. Chem.* **2012**, *22*, 8911–8915. [CrossRef]
62. Lu, Z.; Gao, D.; Yi, D.; Yang, Y.; Wang, X.; Yao, J. $sp^2/sp^3$ hybridized carbon as an anode with extra Li-ion storage capacity: Construction and origin. *ACS Cent. Sci.* **2020**, *6*, 1451–1459. [CrossRef]
63. Yan, J.; Li, W.; Feng, P.; Wang, R.; Jiang, M.; Han, J.; Cao, S.; Wang, K.; Jiang, K. Enhanced $Na^+$ pseudocapacitance in a P, S co-doped carbon anode arising from the surface modification by sulfur and phosphorus with C-S-P coupling. *J. Mater. Chem. A* **2020**, *8*, 422–432. [CrossRef]
64. Gopalakrishnan, A.; Raju, D.; Badhulika, S. Green synthesis of nitrogen, sulfur-co-doped worm-like hierarchical porous carbon derived from ginger for outstanding supercapacitor performance. *Carbon* **2020**, *168*, 209–219. [CrossRef]
65. Li, G.; Mao, K.; Liu, M.; Yan, M.; Zhao, J.; Zeng, Y.; Yang, L.; Wu, Q.; Wang, X.; Hu, Z. Achieving ultrahigh volumetric energy storage by compressing nitrogen and sulfur dual-doped carbon nanocages via capillarity. *Adv. Mater.* **2020**, *32*, 2004632. [CrossRef] [PubMed]
66. Zhao, G.; Yu, D.; Zhang, H.; Sun, F.; Li, J.; Zhu, L.; Sun, L.; Yu, M.; Besenbacher, F.; Sun, Y. Sulphur-doped carbon nanosheets derived from biomass as high-performance anode materials for sodium-ion batteries. *Nano Energy* **2020**, *67*, 104219. [CrossRef]
67. Li, D.; Chang, G.; Zong, L.; Xue, P.; Wang, Y.; Xia, Y.; Lai, C.; Yang, D. From double-helix structured seaweed to S-doped carbon aerogel with ultra-high surface area for energy storage. *Energy Storage Mater.* **2018**, *17*, 22–30. [CrossRef]
68. Casal, M.; Díez, N.; Payá, S.; Sevilla, M. Cork-derived carbon sheets for high-performance Na-ion capacitors. *ACS Appl. Energy Mater.* **2023**, *6*, 8120–8131. [CrossRef] [PubMed]
69. Hong, Z.; Zhen, Y.; Ruan, Y.; Kang, M.; Zhou, K.; Zhang, J.; Huang, Z.; Wei, M. Rational design and general synthesis of S-Doped hard carbon with tunable doping sites toward excellent Na-ion storage performance. *Adv. Mater.* **2018**, *30*, 1802035. [CrossRef]
70. Liu, F.; Niu, J.; Chuan, X.; Zhao, Y. Nitrogen and phosphorus co-doped porous carbon: Dopant, synthesis, performance enhancement mechanism and versatile applications. *J. Power Sources* **2024**, *601*, 234308. [CrossRef]
71. Wang, H.; Chen, H.; Chen, C.; Li, M.; Xie, Y.; Zhang, X.; Wu, X.; Zhang, Q.; Lu, C. Tea-derived carbon materials as anode for high-performance sodium ion batteries. *Chin. Chem. Lett.* **2023**, *34*, 107465. [CrossRef]
72. Liu, H.; Wang, M.; Zhai, D.; Chen, X.; Zhang, Z. Design and theoretical study of carbon-based supercapacitors especially exhibiting superior rate capability by the synergistic effect of nitrogen and phosphor dopants. *Carbon* **2019**, *155*, 223–232. [CrossRef]
73. Wang, X.; Hou, M.; Shi, Z.; Liu, X.; Mizota, I.; Lou, H.; Wang, B.; Hou, X. Regulate phosphorus configuration in high P-doped hard carbon as a superanode for sodium storage. *ACS Appl. Mater. Interfaces* **2021**, *13*, 12059–12068. [CrossRef]
74. Guo, J.; Xu, X.; Hill, J.; Wang, L.; Dang, J.; Kang, Y.; Li, Y.; Guan, W.; Yamauchi, Y. Graphene-carbon 2D heterostructures with hierarchically-porous P, N-doped layered architecture for capacitive deionizatio. *Chem. Sci.* **2021**, *12*, 10334–10340. [CrossRef]
75. Yang, Z.; Gao, Y.; Zhao, Z.; Wang, Y.; Wu, Y.; Wang, X. Phytic acid assisted formation of P-doped hard carbon anode with enhanced capacity and rate capability for lithium ion capacitors. *J. Power Sources* **2020**, *474*, 228500. [CrossRef]

76. Qian, Y.; Jiang, S.; Li, Y.; Yi, Z.; Zhou, J.; Li, T.; Han, Y.; Wang, Y.; Tian, J.; Lin, N.; et al. In situ revealing the electroactivity of P-O and P-C bonds in hard carbon for high-capacity and long-life Li/K-ion batteries. *Adv. Energy Mater.* **2019**, *9*, 1901676. [CrossRef]
77. Li, Y.; Yuan, Y.; Bai, Y.; Liu, Y.; Wang, Z.; Li, L.; Wu, F.; Amine, K.; Wu, C.; Lu, J. Insights into the $Na^+$ storage mechanism of phosphorus-functionalized hard carbon as ultrahigh capacity anodes. *Adv. Energy Mater.* **2018**, *8*, 1702781. [CrossRef]
78. McKee, D. Oxidation protection of carbon materials. In *Chemistry & Physics of Carbon*; CRC Press: Boca Raton, FL, USA, 2021; pp. 173–232. [CrossRef]
79. Yao, J.; Li, F.; Zhou, R.; Guo, C.; Liu, X.; Zhu, Y. Phosphorous-doped carbon nanotube/reduced graphene oxide aerogel cathode enabled by pseudocapacitance for high energy and power zinc-ion hybrid capacitors. *Chin. Chem. Lett.* **2024**, *35*, 108354. [CrossRef]
80. Zhao, Y.; Yang, L.; Chen, S.; Wang, X.; Ma, Y.; Wu, Q.; Jiang, Y.; Qian, W.; Hu, Z. Can boron and nitrogen co-doping improve oxygen reduction reaction activity of carbon nanotubes? *J. Am. Chem. Soc.* **2013**, *135*, 1201–1204. [CrossRef]
81. Kim, Y.; Fujisawa, K.; Muramatsu, H.; Hayashi, T.; Endo, M.; Fujimori, T.; Kaneko, K.; Terrones, M.; Behrends, J.; Eckmann, A.; et al. Raman spectroscopy of boron-doped single-layer graphene. *ACS Nano* **2012**, *6*, 6293–6300. [CrossRef]
82. Zhang, Y.; Zuo, L.; Zhang, L.; Yan, J.; Lu, H.; Fan, W.; Liu, T. Immobilization of NiS nanoparticles on N-doped carbon fiber aerogels as advanced electrode materials for supercapacitors. *Nano Res.* **2016**, *9*, 2747–2759. [CrossRef]
83. Han, J.; Zhang, L.; Lee, S.; Oh, J.; Lee, K.; Potts, J.; Ji, J.; Zhao, X.; Ruoff, R.; Park, S. Generation of B-doped graphene nanoplatelets using a solution process and their supercapacitor application. *ACS Nano* **2013**, *7*, 19–26. [CrossRef]
84. Panchakarla, S.; Subrahmanyam, S.; Saha, K.; Govindaraj, A.; Krishnamurthy, R.; Waghmare, V.; Rao, R. Synthesis, structure, and properties of boron- and nitrogen-doped graphene. *Adv. Mater.* **2009**, *21*, 4726–4730. [CrossRef]
85. Bhattacharjee, U.; Bhowmik, S.; Ghosh, S.; Vangapally, N.; Martha, S. Boron-doped graphene anode coupled with microporous activated carbon cathode for lithium-ion ultracapacitors. *Chem. Eng. J.* **2022**, *430*, 132835. [CrossRef]
86. Wang, X.; Sun, G.; Routh, P.; Kim, D.; Huang, W.; Chen, P. Heteroatom-doped graphene materials: Syntheses, properties and applications. *Chem. Soc. Rev.* **2014**, *43*, 7067–7098. [CrossRef] [PubMed]
87. Naresh, V.; Bhattacharjee, U.; Martha, K. Boron doped graphene nanosheets as negative electrode additive for high-performance lead-acid batteries and ultracapacitors. *J. Alloys Compd.* **2019**, *797*, 595–605. [CrossRef]
88. Miao, X.; Sun, D.; Zhou, X.; Lei, Z. Designed formation of nitrogen and sulfur dual-doped hierarchically porous carbon for long-life lithium and sodium ion batteries. *Chem. Eng. J.* **2019**, *364*, 208–216. [CrossRef]
89. Ruan, J.; Zhao, Y.; Luo, S.; Yuan, T.; Yang, J.; Sun, D.; Zheng, S. Fast and stable potassium-ion storage achieved by in situ molecular self-assembling N/O dual-doped carbon network. *Energy Storage Mater.* **2019**, *23*, 46–54. [CrossRef]
90. Zou, G.; Hou, H.; Foster, C.; Banks, C.; Guo, T.; Jiang, Y.; Zhang, Y.; Ji, X. Advanced hierarchical vesicular carbon co-doped with S, P, N for high-rate sodium storage. *Adv. Sci.* **2018**, *5*, 1800241. [CrossRef]
91. Huang, R.; Cao, Y.; Qin, S.; Ren, Y.; Lan, R.; Zhang, L.; Yu, Z.; Yang, H. Ultra-high N-doped open hollow carbon nano-cage with excellent $Na^+$ and $K^+$ storage performances. *Mater. Today Nano* **2022**, *18*, 100217. [CrossRef]
92. Hu, S.; Ge, Z.; Tan, J.; Lai, H.; Feng, T.; Zhang, S.; Xu, Z.; Zhou, H.; Cao, X.; Zhu, G.; et al. Dual-functionally modified N/S doped hierarchical porous carbon and glycerol-engineered polyacrylonitrile carbon nanofibers combine for high-performance lithium-ion capacitors. *J. Power Sources* **2023**, *558*, 232624. [CrossRef]
93. Guan, L.; Pan, L.; Peng, T.; Gao, C.; Zhao, W.; Yang, Z.; Hu, H.; Wu, M. Synthesis of biomass-derived nitrogen-doped porous carbon nanosheests for high-performance supercapacitors. *ACS Sustain. Chem. Eng.* **2019**, *7*, 8405–8412. [CrossRef]
94. Pei, Z.; Li, H.; Huang, Y.; Xue, Q.; Huang, Y.; Zhu, M.; Wang, Z.; Zhi, C. Texturing in situ: N, S-enriched hierarchically porous carbon as a highly active reversible oxygen electrocatalyst. *Energy Environ. Sci.* **2017**, *10*, 742–749. [CrossRef]
95. Ghosh, S.; Barg, S.; Jeong, S.; Ostrikov, K. Heteroatom-doped and oxygen-functionalized nanocarbons for high-performance supercapacitors. *Adv. Energy Mater.* **2020**, *10*, 2001239. [CrossRef]
96. Chen, M.; Le, T.; Zhou, Y.; Kang, F.; Yang, Y. Thiourea-induced N/S dual-doped hierarchical porous carbon nanofibers for high-performance lithium-ion capacitors. *ACS Appl. Energy Mater.* **2020**, *3*, 1653–1664. [CrossRef]
97. Hu, L.; Hou, J.; Ma, Y.; Li, H.; Zhai, T. Multi-heteroatom self-doped porous carbon derived from swim bladders for large capacitance supercapacitors. *J. Mater. Chem. A* **2016**, *4*, 15006–15014. [CrossRef]
98. Wang, J.; Liu, H.; Zhang, X.; Shao, M.; Wei, B. Elaborate construction of N/S-co-doped carbon nanobowls for ultrahigh-power supercapacitors. *J. Mater. Chem. A* **2018**, *6*, 17653–17661. [CrossRef]
99. Xu, F.; Tang, Z.; Huang, S.; Chen, L.; Liang, Y.; Mai, W.; Zhong, H.; Fu, R.; Wu, D. Facile synthesis of ultrahigh-surface-area hollow carbon nanospheres for enhanced adsorption and energy storage. *Nat. Commun.* **2015**, *6*, 7221. [CrossRef] [PubMed]
100. Xu, D.; Chen, C.; Xie, J.; Zhang, B.; Miao, L.; Cai, J.; Huang, Y.; Zhang, L. A hierarchical N/S-codoped carbon anode fabricated facilely from cellulose/polyaniline microspheres for high-performance sodium-ion batterie. *Adv. Energy Mater.* **2016**, *6*, 1501929. [CrossRef]
101. Ye, J.; Zang, J.; Tian, Z.; Zheng, M.; Dong, Q. Sulfur and nitrogen co-doped hollow carbon spheres for sodium-ion batteries with superior cyclic and rate performance. *J. Mater. Chem. A* **2016**, *4*, 13223–13227. [CrossRef]

102. Chen, C.; Li, G.; Zhu, J.; Lu, Y.; Jiang, M.; Hu, Y.; Shen, Z.; Zhang, X. In-situ formation of tin-antimony sulfide in nitrogen-sulfur co-doped carbon nanofibers as high performance anode materials for sodium-ion batteries. *Carbon* **2017**, *120*, 380–391. [CrossRef]
103. Sheng, J.; Yang, L.; Zhu, Y.; Li, F.; Zhang, Y.; Zhou, Z. Oriented SnS nanoflakes bound on S-doped N-rich carbon nanosheets with a rapid pseudocapacitive response as high-rate anodes for sodium-ion batteries. *J. Mater. Chem. A* **2017**, *5*, 19745–19751. [CrossRef]
104. Zou, L.; Lai, Y.; Hu, H.; Wang, M.; Zhang, K.; Zhang, P.; Fang, J.; Li, J. N/S Co-doped 3D porous carbon nanosheet networks enhancing anode performance of sodium-ion batteries. *Chem. A Eur. J.* **2017**, *23*, 14261–14266. [CrossRef]
105. Ruan, J.; Yuan, T.; Pang, Y.; Luo, S.; Peng, C.; Yang, J.; Zheng, S. Nitrogen and sulfur dual-doped carbon films as flexible free-standing anodes for Li-ion and Na-ion batteries. *Carbon* **2018**, *126*, 9–16. [CrossRef]
106. Yang, J.; Zhou, X.; Wu, D.; Zhao, X.; Zhou, Z. S-doped N-rich carbon nanosheets with expanded interlayer distance as anode materials for sodium-ion batteries. *Adv. Mater.* **2017**, *29*, 1604108. [CrossRef]
107. Xu, Y.; Jiang, J.; Li, Z.; Yang, Z.; Zhang, Y.; An, Y.; Zhu, Q.; Dou, H.; Zhang, X. Aerosol-assisted preparation of N-doped hierarchical porous carbon spheres cathodes toward high-stable lithium-ion capacitors. *J. Mater. Sci.* **2020**, *55*, 13127–13140. [CrossRef]
108. Sun, L.; Zhou, H.; Yao, Y.; Qu, H.; Zhang, C.; Liu, S.; Zhou, Y. Double soft-template synthesis of nitrogen/sulfur-codoped hierarchically porous carbon materials derived from protic ionic liquid for supercapacitor. *ACS Appl. Mater. Interfaces* **2017**, *9*, 26088–26095. [CrossRef] [PubMed]
109. Deng, X.; Zou, K.; Momen, R.; Cai, P.; Chen, J.; Hou, H.; Zou, G.; Ji, X. High content anion (S/Se/P) doping assisted by defect engineering with fast charge transfer kinetics for high-performance sodium ion capacitors. *Sci. Bull.* **2021**, *66*, 1858–1868. [CrossRef] [PubMed]
110. Shi, L.; Zeng, Q.; Liu, J.; Yang, Y. S, N co-doped porous carbon derived from metal-organic frameworks as cathode for lithium-ion capacitor. *J. Electroanal. Chem.* **2023**, *944*, 117675. [CrossRef]
111. Bhagwan, J.; Nagaraju, G.; Ramulu, B.; Sekhar, S.; Yu, J. Rapid synthesis of hexagonal $NiCo_2O_4$ nanostructures for high-performance asymmetric supercapacitors. *Electrochim. Acta* **2019**, *299*, 509–517. [CrossRef]
112. Gu, J.; Sun, L.; Zhang, Y.; Zhang, Q.; Li, X.; Si, H.; Shi, Y.; Sun, C.; Gong, Y.; Zhang, Y. MOF-derived Ni-doped CoP@C grown on CNTs for high-performance supercapacitors. *Chem. Eng. J.* **2020**, *385*, 123454. [CrossRef]
113. Zou, K.; Deng, W.; Silvester, D.S.; Zou, G.; Hou, H.; Banks, C.E.; Li, L.; Hu, J.; Ji, X. Carbonyl chemistry for advanced electrochemical energy storage systems. *ACS Nano* **2024**, *18*, 19950–20000. [CrossRef]
114. Hu, Y.; Tang, C.; Li, H.; Du, A.; Luo, W.; Wu, M.; Zhang, H. B-incorporated, N-doped hierarchically porous carbon nanosheets as anodes for boosted potassium storage capability. *Chin. Chem. Lett.* **2022**, *33*, 480–485. [CrossRef]
115. Choi, C.H.; Park, S.H.; Woo, S.I. Binary and ternary doping of nitrogen, boron, and phosphorus into carbon for enhancing electrochemical oxygen reduction activity. *ACS Nano* **2012**, *6*, 7084–7091. [CrossRef]
116. Wang, S.; Iyyamperumal, E.; Roy, A.; Xue, Y.; Yu, D.; Dai, L. Vertically aligned BCN nanotubes as efficient metal-free electrocatalysts for the oxygen reduction reaction: A synergetic effect by co-doping with boron and nitrogen. *Angew. Chem. Int. Ed.* **2011**, *50*, 11756–11760. [CrossRef]
117. Zheng, Y.; Jiao, Y.; Ge, L.; Jaroniec, M.; Qiao, S. Two-step boron and nitrogen doping in graphene for enhanced synergistic catalysis. *Angew. Chem. Int. Ed.* **2013**, *52*, 3110–3116. [CrossRef] [PubMed]
118. Wu, Z.; Winter, A.; Chen, L.; Sun, Y.; Turchanin, A.; Feng, X.; Müllen, K. Three-dimensional nitrogen and boron co-doped graphene for high-performance all-solid-state supercapacitors. *Adv. Mater.* **2012**, *24*, 5130–5135. [CrossRef]
119. Zhang, H.; Hu, M.; Huang, Z.; Kang, F.; Lv, R. Sodium-ion capacitors with superior energy-power performance by using carbon-based materials in both electrodes. *Prog. Nat. Sci. Mater. Int.* **2020**, *30*, 13–19. [CrossRef]
120. Putri, K.; Ong, W.; Chang, S.; Chai, S. Heteroatom doped graphene in photocatalysis: A review. *Appl. Surf. Sci.* **2015**, *358*, 2–14. [CrossRef]
121. Subramanyan, K.; Divya, M.; Aravindan, V. Dual-carbon Na-ion capacitors: Progress and future prospects. *J. Mater. Chem. A* **2021**, *9*, 9431–9450. [CrossRef]
122. Li, S.; Liu, P.; Zheng, X.; Wu, M. High-performance dual carbon lithium-ion capacitors based on nitrogen-doped 2D carbon nanosheets as both anode and cathode. *Electrochim. Acta* **2022**, *428*, 140921. [CrossRef]
123. Jiang, J.; Shen, Q.; Chen, Z.; Wang, S. Nitrogen-doped porous carbon derived from coal for high-performance dual-carbon lithium-ion capacitors. *Nanomaterials* **2023**, *13*, 2525. [CrossRef] [PubMed]
124. Jiang, J.; Zhang, Y.; An, Y.; Wu, L.; Zhu, Q.; Dou, H.; Zhang, X. Engineering ultrathin $MoS_2$ nanosheets anchored on N-doped carbon microspheres with pseudocapacitive properties for high-performance lithium-ion capacitors. *Small Methods* **2019**, *3*, 1900081. [CrossRef]
125. Xiao, Z.; Yu, Z.; Gao, Z.; Li, B.; Zhang, M.; Xu, C. S-doped graphene nano-capsules toward excellent low-temperature performance in Li-ion capacitors. *J. Power Sources* **2022**, *535*, 231404. [CrossRef]
126. Thangavel, R.; Kannan, G.; Ponraj, R.; Yoon, G.; Aravindan, V.; Kim, D.; Kang, K.; Yoon, W.; Lee, Y. Surface enriched graphene hollow spheres towards building ultra-high power sodium-ion capacitor with long durability. *Energy Storage Mater.* **2019**, *25*, 702–713. [CrossRef]

127. Zou, G.; Hou, H.; Zhao, G.; Huang, Z.; Ge, P.; Ji, X. Preparation of S/N-codoped carbon nanosheets with tunable interlayer distance for high-rate sodium-ion batteries. *Green Chem.* **2017**, *19*, 4622–4632. [CrossRef]
128. Dong, S.; Xu, Y.; Wu, L.; Dou, H.; Zhang, X. Surface-functionalized graphene-based quasi-solid-state Na-ion hybrid capacitors with excellent performance. *Energy Storage Mater.* **2018**, *11*, 8–15. [CrossRef]
129. Du, Q.; Zhao, Y.; Chen, Y.; Liu, J.; Li, H.; Bai, G.; Zhou, K.; Wang, J. Nitrogen-doped porous carbon nanosheets as both anode and cathode for advanced potassium-ion hybrid capacitors. *Green Energy Environ.* **2023**, *8*, 579–588. [CrossRef]
130. Zhang, W.; Yin, J.; Sun, M.; Wang, W.; Chen, C.; Altunkaya, M.; Emwas, A.; Han, Y.; Schwingenschlögl, U.; Alshareef, H. Direct pyrolysis of supermolecules: An ultrahigh edge-nitrogen doping strategy of carbon anodes for potassium-ion batteries. *Adv. Mater.* **2020**, *32*, 2000732. [CrossRef] [PubMed]
131. Pham, H.; Mahale, K.; Hoang, T.; Mundree, S.; Gomez-Romero, P.; Dubal, D. Dual carbon potassium-ion capacitors: Biomass-derived graphene-like carbon nanosheet cathodes. *ACS Appl. Mater. Interfaces* **2020**, *12*, 48518–48525. [CrossRef]
132. Hu, X.; Liu, Y.; Chen, J.; Yi, L.; Zhan, H.; Wen, Z. Fast redox kinetics in Bi-heteroatom doped 3D porous carbon nanosheets for high-performance hybrid potassium-ion battery capacitors. *Adv. Energy Mater.* **2019**, *9*, 1901533. [CrossRef]
133. Chang, X.; Zhou, X.; Ou, X.; Lee, C.; Zhou, J.; Tang, Y. Ultrahigh nitrogen doping of carbon nanosheets for high capacity and long cycling potassium ion storage. *Adv. Energy Mater.* **2019**, *9*, 1902672. [CrossRef]
134. Tai, Z.; Liu, Y.; Zhang, Q.; Zhou, T.; Guo, Z.; Liu, H.K.; Dou, S.X. Ultra-light and flexible pencil-trace anode for high performance potassium-ion and lithium-ion batteries. *Green Energy Environ.* **2017**, *2*, 278–284. [CrossRef]
135. Tan, L.; Huang, X.; Yin, T.; Guo, Y.; Ning, T.; Mei, Y.; Zou, K.; Li, L.; Ji, X.; Zou, G. A 5 V ultrahigh energy density lithium metal capacitor enabled by the fluorinated electrolyte. *Energy Storage Mater.* **2024**, *71*, 103692. [CrossRef]
136. Cao, J.; Xu, H.; Zhong, J.; Li, X.; Li, S.; Wang, Y.; Zhang, M.; Deng, H.; Wang, Y.; Cui, C.; et al. Dual-carbon electrode-based high-energy-density potassium-ion hybrid capacitor. *ACS Appl. Mater. Interfaces* **2021**, *13*, 8497–8506. [CrossRef] [PubMed]
137. Cui, Y.; Liu, W.; Wang, X.; Li, J.; Zhang, Y.; Du, Y.; Liu, S.; Wang, H.; Feng, W.; Chen, M. Bioinspired mineralization under freezing conditions: An approach to fabricate porous carbons with complicated architecture and superior $K^+$ storage performance. *ACS Nano* **2019**, *13*, 11582–11592. [CrossRef] [PubMed]
138. Gao, Y.; Yang, Z.; Wang, Y.; Wang, X. Boosting capacitive storage of cathode for lithium-ion capacitors: Combining pore structure with P-doping. *Electrochim. Acta* **2021**, *368*, 137646. [CrossRef]
139. Huynh, N.; Tran, D.; Nguyen, A.; Nguyen, T.; Tran, M.; Grag, A.; Le, P. Carbon-coated $LiFePO_4$-carbon nanotube electrodes for high-rate Li-ion battery. *J. Solid State Electrochem.* **2018**, *22*, 2247–2254. [CrossRef]
140. Shah, A.; Zahid, A.; Subhan, H.; Munir, A.; Iftikhar, F.; Akbar, M. Heteroatom-doped carbonaceous electrode materials for high performance energy storage devices. *Sustain. Energy Fuels* **2018**, *2*, 1398–1429. [CrossRef]
141. Qi, C.; Ma, X.; Ning, G.; Song, X.; Chen, B.; Lan, X.; Li, Y.; Zhang, X.; Gao, J. Aqueous slurry of S-doped carbon nanotubes as conductive additive for lithium ion batteries. *Carbon* **2015**, *92*, 245–253. [CrossRef]
142. Zhao, L.; Sun, D.; Cao, Q.; Xiao, Z.; Yu, Z.; Qi, C.; Li, X.; Ning, G.; Ma, X.; Peng, C.; et al. Green and universal sulfur doping technique coupled with construction of conductive network for enhanced kinetics of Li-ion capacitors. *Chem. Eng. Sci.* **2022**, *258*, 117749. [CrossRef]
143. Yang, C.; Xiong, J.; Ou, X.; Wu, C.; Xiong, X.; Wang, J.; Huang, K.; Liu, M. A renewable natural cotton derived and nitrogen/sulfur co-doped carbon as a high-performance sodium ion battery anode. *Mater. Today Energy* **2018**, *8*, 37–44. [CrossRef]
144. Zou, K.; Cai, P.; Liu, C.; Li, J.; Gao, X.; Xu, L.; Zou, G.; Hou, H.; Liu, Z.; Ji, X. A kinetically well-matched full-carbon sodium-ion capacitor. *J. Mater. Chem. A* **2019**, *7*, 13540–13549. [CrossRef]
145. Que, L.; Yu, F.; He, K.; Wang, Z.; Gu, D. Robust and conductive $Na_2Ti_2O_{5-x}$ nanowire arrays for high-performance flexible sodium-ion capacitor. *Chem. Mater.* **2017**, *29*, 9133–9141. [CrossRef]
146. Wang, C.; Zhao, N.; Li, B.; Yu, Q.; Shen, W.; Kang, F.; Lv, R.; Huang, Z. Pseudocapacitive porous hard carbon anode with controllable pyridinic nitrogen and thiophene sulfur co-doping for high-power dual-carbon sodium ion hybrid capacitors. *J. Mater. Chem. A* **2021**, *9*, 20483–20492. [CrossRef]
147. Liu, Z.; Peng, H.; Xie, X.; Wang, X.; Hou, W.; Miao, W.; Tao, B.; Ma, G.; Lei, Z. Coupling of reasonable micro-defect structure and multiple chemisorption sites for boosting the $K^+$ storage capacity in dual-carbon potassium ion hybrid capacitors. *Energy Storage Mater.* **2024**, *65*, 103100. [CrossRef]
148. Peng, Z.; Bannov, G.; Li, S.; Huang, Y.; Tang, L.; Tan, L.; Chen, Y. Coupling uniform pore size and multi-chemisorption sites: Hierarchically ordered porous carbon for ultra-fast and large zinc ion storage. *Adv. Funct. Mater.* **2023**, *33*, 2303205. [CrossRef]


**Disclaimer/Publisher's Note:** The statements, opinions and data contained in all publications are solely those of the individual author(s) and contributor(s) and not of MDPI and/or the editor(s). MDPI and/or the editor(s) disclaim responsibility for any injury to people or property resulting from any ideas, methods, instructions or products referred to in the content.